UNIVERSITY OF NAPLES FEDERICO II

DOCTORATE IN
MOLECULAR MEDICINE AND MEDICAL BIOTECHNOLOGY

XXXIII CYCLE

Federica Aliotta

BIOCHEMICAL STUDIES OF A NOVEL CLASS OF CDC25 INHIBITORS AND BIOLOGICAL ANALYSIS OF THE EFFECT IN MELANOMA CELL LINES

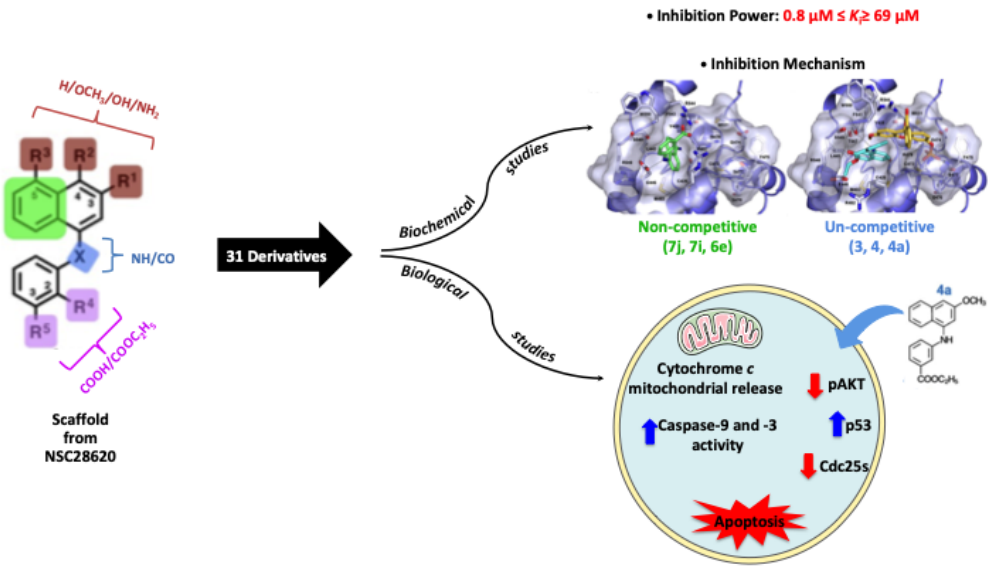

Year 2021

UNIVERSITY OF NAPLES FEDERICO II

DOCTORATE IN
MOLECULAR MEDICINE AND MEDICAL BIOTECHNOLOGY

XXXIII CYCLE

BIOCHEMICAL STUDIES OF A NOVEL CLASS OF CDC25 INHIBITORS AND BIOLOGICAL ANALYSIS OF THE EFFECT IN MELANOMA CELL LINES

Tutor
Prof. Maria Rosaria Ruocco

Candidate
Federica Aliotta

Year 2021

INDEX

ABBREVIATIONS

BSA	bovine serum albumin
Cdc25	cell division cycle 25
Cdk	cyclin-dependent kinase
DMEM	Dulbecco's modified Eagle's medium
DMSO	dimethyl sulfoxide
FBS	foetal bovine serum
MTT	3-(4,5-dimethylthiazol-2-yl)-2,5-diphenyltetrazolium bromide
NPA	naphthylphenylamine
NPK	naphthylphenylketone
OMFP	3-O-methylfluorescein phosphate
PBS	phosphate-buffered saline
PDB	protein data bank
PI	propidium iodide
ROS	reactive oxygen species
SDS/PAGE	sodium dodecyl sulfate polyacrylamide gel electrophoresis
TCEP	tris-(2-carboxyethyl)-phosphine hydrochloride

ABSTRACT

Cell division cycle 25 (Cdc25) phosphatases play a pivotal role in the regulation of cell cycle. Because of their altered expression in some tumors, Cdc25s are considered promising targets for cancer therapy. Previously my research group demonstrated that the compound **NSC28620** acts as a reversible inhibitor of Cdc25s and affects the cell viability of some cancer cell lines at 200 μM. To identify more potent inhibitors of Cdc25s, thirty-one **NSC28620** derivatives were characterized. From kinetic measurements of the phosphatase activity sustained by the recombinant form of Cdc25B emerged that some derivatives (**7j**, **7i**, **6e**, **7f**, and **3**) showed a higher inhibitory activity compared to the lead **NSC28620**, with the most potent inhibitor **7j** (K_i, 0.8 μM). Intrinsic fluorescence measurements, performed to study the Cdc25B•inhibitor interaction, ranked the thirty-one derivatives in two main groups of inhibitors, i.e. noncompetitive, uncompetitive. Biological study revealed that only one derivative, compound **4a**, exerted a specific toxic action in melanoma cells, at lower concentration (5-10 μM) respect to the lead compound. Cytofluorimetric analysis indicated that this molecule arrests the cells in G2/M phase and induces apoptosis. In particular, fluorimetric measurements of caspase-3 and -9 activity and western blotting analysis of sub-cellular localization of cytochrome *c* suggest that **4a** activates an apoptotic program, mainly mitochondria and caspase-mediated. Furthermore, **4a** reduces the protein levels of all three forms of Cdc25 and affects the expression of typical proliferation and apoptotic markers, such as pAkt and p53.

In the complex, the discovery and production of more potent bioactive molecules can contribute to the advancement of research on new therapeutic strategies against one of the most deadly tumors such as melanoma.

1. INTRODUCTION

1.1 Cdc25 enzymes

In the 1986 Russel and Nurse, through experiments on fission yeast, identified for the first time a factor required to entry into mitosis, named Cell Division Cycle 25 (Cdc25). Nowadays, it is known that Cdc25 enzymes are expressed in all eukaryotes except plants and in mammals there are three forms of Cdc25 (Cdc25A, Cdc25B and Cdc25B) (Galaktionov et al. 1995; Boudolf et al. 2006). Cdc25s are phosphatases involved in the regulation of cell cycle progression (Sur & Agrawal 2016). All cells must provide a fine control of the cell cycle in order to transmit to daughter cells a faithful copy of their genome. Cyclin-dependent kinases (Cdks) represent the main actors in the regulation of cell cycle. Hence, Cdks are controlled by a variety of positive and negative mechanisms. For example, Cdk1 and Cdk2, expressed constantly during the cell cycle, are activated through the binding of the cyclin subunit and the phosphorylation of a specific threonine residue in a domain called T-loop. Instead, the phosphorylation of Cdk1 and Cdk2 by Wee1/Mik1/Myt1, of other two amino acid residues, *i.e.* Tyr15 and Thr14, provides their inactivation. On the other hand, the dephosphorylation of these tyrosine and threonine residues by Cdc25s induces the activation of Cdks. Indeed, Cdc25s are dual phosphatases that can dephosphorylate phosphotyrosine and phosphothreonine residues, in order to activate their Cdk substrates. All Cdc25s have a similar structure. Their lengths range between 423 and 566 amino acids. The N-terminal region consists in the regulatory moiety of the proteins because of the presence of sites for phosphorylation, ubiquitination and proline isomerization. This region is divergent in the three forms of Cdc25, showing approximately 20% of homology. The C-terminal region, highly homologous in the Cdc25s, contains the catalytic domain, which can dephosphorylate protein substrate, and one site of phosphorylation (Thr507). The catalytic domain contains the HCX_5R motif, characteristic of all protein tyrosine phosphatases. “C”

represents the catalytic cysteine instead the five "X" are the amine backbone and "R" is the arginine, these last two parts form the loop that bind the phosphate. However, the C-terminal region contains a regulatory site too, in particular, a phosphorylation site for Chk1 (Thr50), that maybe is responsible of the control by 14-3-3 proteins and cyclin B binding during mitosis (Kristjànsdòttir & Rudolph 2004). The different forms of Cdc25 target different Cdks (Figure 1). Cdc25B and Cdc25C dephosphorylate the complexes Cdk2/cyclinA, Cdk1/cyclinA and Cdk1/cyclinB regulating the G2/M transition, whereas Cdc25A triggers both the G1/S and G2/M progressions (Kristjànsdòttir & Rudolph 2004; Rudolph 2007). In particular, Cdc25A during the G1/S transition activates Cdk4/cyclinD, Cdk2/cyclinE and Cdk6/cyclinD complexes, through Cdk dephosphorylation. These events result in the association of pRb (phosphorylate retinoblastoma protein) with E2F transcription factor that promotes the expression of genes necessary for the progression of the cell cycle (Shen & Huang 2012). Moreover, during S phase the synergic action of Cdc25A and Cdc25B actives the complex Cdk2/cyclinA which in turn actives proteins requested for DNA replication. Cdc25B plays a role also in the late S phase dephosphorylating Cdk1/cyclinA (Brenner et al. 2014). In the G2/M transition all the three forms of Cdc25 are involved. The main actor of the mitosis process is the Cdk1/cyclinB complex that is presumed to trigger the mitotic spindle formation and the centrosome separation. Cdc25B is the started activator of Cdk1/cyclinB complex that is definably activated by Cdc25C at the beginning of the mitosis in the nucleus. Instead Cdc25A has the role to phosphorylate and stabilize the active form of Cdk1/cyclinB. When the mitosis ends the APC/C-dependent ubiquitination of Cdk1/cyclinB and CDC25s leads to their proteasome-mediated degradation (Boutros et al. 2006; Boutros et al. 2007; Lindqvist et al. 2005; Suryadinata et al. 2010). However, remain unclear the specific role of each Cdc25 form in the cell cycle control because it has been shown that the lack of one of the three forms of Cdc25 is not critical for viability.

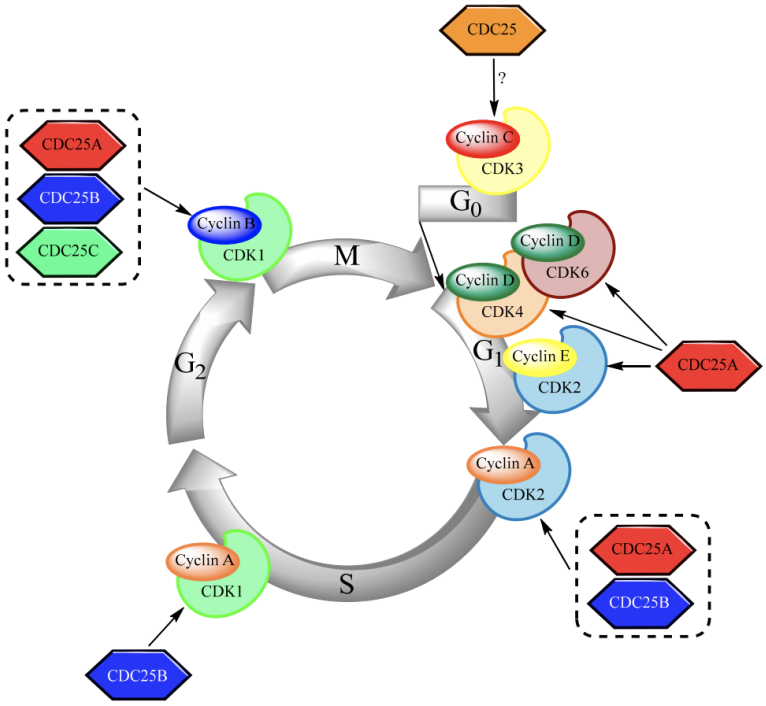

Figure 1. Regulatory function of Cdc25s in the cell cycle progression. An overview of the regulatory function of Cdc25s in cell cycle progression. At G0-phase, cells that had been quiescent, re-enter the cell cycle after activation of CDK3/cyclin C. Dephosphorylation of CDK4/cyclin D, CDK6/cyclin D and CDK2 both in complex with cyclin E and cyclin A by Cdc25s leads to the transition into the DNA-replication phase. At late S-phase, Cdc25B activates CDK1/cyclin A. Finally, dephosphorylation of CDK1/cyclin B triggers mitotic entry, and in this important step all three Cdc25 isoforms are involved. At the end of mitosis, both CDK1/cyclin B and the Cdc25s are degraded and the cycle can start all over again *(Brenner et al. Molecules 2014).*

Indeed, knock-out mice for Cdc25C or B show a normal development. It is hypothesized that each Cdc25 form can balance and compensate the deficiency of the other forms (Chen et al. 2001; Lincoln et al. 2002). Cdc25 enzymes are also involved in the cell response to the DNA damage induced by ultraviolet light (UV), ionizing irradiation (IR) and other DNA damage agents (Figure 2). The IR induces the cells to trigger the ATM (ataxia-telangiectasia mutated) and/or ATR (ATM- and Rad3-Related) pathways. ATM and ATR are kinases that regulate the network of cellular mechanisms aimed at maintaining genomic integrity. In particular, ATM is activated only by double-strand DNA breaks (DSBs), instead ATR is sensible to a wide variety of DNA damages. The

action of ATM and ATR leads to the activation of checkpoint kinases (Chk1 and Chk2), which in turn induces the inhibition and finally the degradation of the Cdc25s, resulting in the arrest of the cell cycle, until the DNA lesion is fixed. If the damage is irreversible the cell activates the apoptotic program (McGowan et al. 2004; Maréchal & Zou 2013). The cell cycle progression can be arrested in three points: at the G1/S transition, during the S phase, and before the beginning of mitosis, at the G2/M transition. At the first checkpoint, G1/S transition, ATM actives Chk2 and ATR actives Chk1. Activated Chk1 and Chk2 arrest the cell cycle through the phosphorylation of Cdc25A that provokes both its exit from the nucleus and degradation. During the S phase the arrest of cell cycle is induced by ATM and ATR through the inactivation of Cdc25A and the maintenance of Cdk2 in the inactive form (Niida & Nakanishi 2006; Sancar at al. 2004). During G2/M transition, Chk1 activation mediates the inactivation of all three forms of Cdc25, thus provoking a block of cell cycle progression (Kristjànsdòttir & Rudolph 2004; Rudolph 2007). Along with ATM and ATR, there are other effectors that act on Cds25s in order to arrest the cell cycle in case of DNA damage, such as MAPKs and PI3K/Akt. Cdc25B and Cdc25A are phosphorylated by MAPKAP kinases 2, whereas Cdc25C is phosphorylated by Chk2 (Kiyokawa et al. 2012; Serçin & Kemp 2011). In response to DNA damage provoked by irradiation, oxidative stress, starvation and heat shock MAPKs pathway downregulates Cdc25s (Rezatabar et al. 2019). Akt promotes Cdc25s degradation by mediating the binding to 14-3-3 proteins and blocking the cell cycle. On the other hand, Akt can provoke the opposite effect through the inactivation of Chk1 and Chk2 allowing the progression of the cell cycle and the survival of cells with damaged genome (Chen et al. 2009; Szymonowicz et al. 2018). These data shows that the pathways that supervise the progression of the cell cycle in response to diverse stimuli constitute a very complex network.

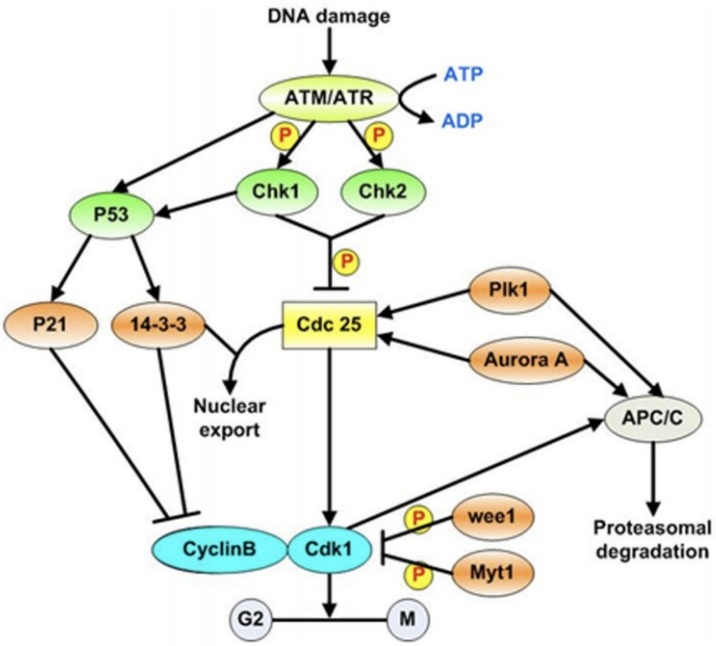

Figure 2. Activation of the G2/M checkpoint after DNA damage. In response to DNA damage, the ATM, ATR signaling pathway is activated, which leads to the phosphorylation and activation of Chk1 and Chk2 and to the subsequent phosphorylation of Cdc25. Phosphorylated Cdc25 is sequestered in the cytoplasm by 14-3-3 proteins, which prevents activation of cyclinB/Cdk1 by Cdc25 and results in G2 arrest. Activated ATM/ATR also activates p53-dependent signaling. This contributes to the maintenance of G2 arrest by upregulating 14-3-3, which sequesters Cdk1 in the cytoplasm. In addition, p53 induces the transactivation of p21, a Cdk inhibitor that binds to and inhibits cyclinB/Cdk1 complexes. P: phosphorylation *(Wang Y. et al., Molecular Cancer, 8, 2009)*.

1.2 Cdc25 and cancer

Although each type of cancer has different origins and traits, some features are common to all tumors. Indeed, the neoplasms are characterized by disorders in the regulation of the cell cycle, leading to uncontrolled cell growth. The disorders in the progression of the cell cycle result from deletions, mutations or deregulation of molecules involved in the control this process. When the cell cycle checkpoint systems are defective the DNA damage remains and thus the DNA mutations are inherited by daughter cells. Under this condition the

genomic instability, which is one on the main features of cancer disorders, takes place. Central regulators of the cell cycle progression are the Cdks and their regulatory subunit, cyclins. A variety of Cdk/cyclin complexes are activated and inactivated by following specific interactions and timing, thus regulating the progression of the cell cycle. In particular, the Cdk/cyclin complexes are activated and inactivated by the addition or removal of phosphates on specific amino acidic residues. Cdc25 enzymes activate Cdk complexes by removing the inhibitory phosphates from tyrosine and threonine residues on Cdks and allowing the progression of the cell cycle. Cdc25s don't play only a role in the regulation of cell cycle but also during the response to DNA damage. Hence, the alteration of Cdc25s activity leads to the accumulation of chromosome abnormalities and could contribute to cancer progression (Kristjànsdòttir & Rudolph 2004; Rudolph 2007; Sur & Agrawal 2016).

The overexpression of Cdc25A, Cdc25B and/or Cdc25C has been demonstrated in various pathological conditions, such as cancers. The altered expression of Cdc25 enzymes has been observed in different type of human tumors and often is associated to poor clinical prognosis. The mechanisms leading to the overexpression of the Cdc25s in the tumor development are still unclear. It is unknown if the Cdc25s overexpression is due to mutations or results from defects at transcription, translation and/or post-translation level (Kristjànsdòttir & Rudolph 2004; Rudolph 2007, Sato et al. 2001, Kiyokawa & Ray 2008).

All the three forms of Cdc25 are involved in the development of different type of tumours. Cdc25A is considered an oncogene and it is mainly localized in the nucleus. This form is overexpressed in a wide range of cancers, such as breast cancer, non-small cell lung cancer, head and neck cancers, and non-Hodgkins lymphoma (Gabrielli & Burgess 2016). The cell cycle–promoting action of Cdc25A is tightly controlled in normal cells and its mis-regulation may result

in aberrantly high Cdk activity. Under physiological condition, the activity of Cdc25A is regulated through the switch from a labile to stable state. In interphase, Cdc25A is associated with the ubiquitin-dependent degradation that keeps the protein in unstable state, whereas during the enter into mitosis, Cdc25A is stabilized by the uncoupling from ubiquitin. Maybe the stable state is ensured by mitosis-specific phosphorylation events that lead to the complete activation of Cdc25A. During the mitosis Cdc25A is phosphorylated by Cdk1/cyclinB complex that prevent the ubiquitin-dependent degradation. The activated Cdc25A, together with Cdc25B and Cdc25C, increase the activity of Cdk1/cyclinB regulating the G2/M transition. During G1 phase, Cdc25A actives Cdk2 through its dephosphorilation, supporting the G1/S progression. Hence, when Cdc25A is overexpressed occurs the deregulation of the G1/S and G2/M transition (Sur & Agrawal 2016). Moreover, the oncogenic role of Cdc25A is also due to its anti-apoptotic role (Zou et al. 2001). In many tumors, the up-regulation of Cdc25A is due to posttranscriptional modifications, provoking an increase of protein stability. However, the oncogenic activity of Cdc25A is observed in association with mutations in other two oncogenes, such as H-Ras and Rb (Gabrielli & Burgess 2016). The Myc transcription factor activates the Cdc25A protein expression. High levels of both Myc and Cdc25A are observed in many tumors (Sur & Agrawal 2016). Hence, the up-regulation of Cdc25A leads to an accelerated entrance into S phase and mitosis (Sexl et al. 1999; Blomberg & Hoffmann 1999).

Also, Cdc25B shows oncogenic features and its overexpression is detected in different cancers, such as colorectal carcinoma, breast cancer, ovarian cancer and neuroblastoma (Kristjansdottir & Rudolph 2004). The expression of Cdc25B is often associated with patient poor prognosis. Cdc25B moves between nucleus and cytoplasm exerting its action in correlation to its cell location. Cdc25B contains two localization signals, one between the amino residues 335-353, the nuclear localization signal (NLS), and another one between the residues 28-40, nucleus export sequence (NES). Cdc25B is

localized into the nucleus during the interphase of cell cycle, while at end of G2 phase, it moves to the cytoplasm where activates Cdk1/cyclinB and contributes to mitosis (Lindqvist et al. 2005). Indeed, mitosis is blocked in the absence of Cdc25B since both Cdc25C and Cdc25B are required for full activation of Cdk1/cyclinB in the G2 phase. The translocation and the inactivation of Cdc25B is regulated by the binding to 14-3-3 proteins. Furthermore, several proteins contribute to regulate the activity of Cdc25B through phosphorylation and dephosphorylation processes. Aurora-A kinase protein phosphorylates Cdc25B by promoting the entry into mitosis. In the course of DNA damage, Aurora-A kinase is inactivated and does not phosphorylate Cdc25B with consequent arrest of the cell cycle (Deibler & Kirschner 2010; Dutertre et al. 2004; Cazales et al. 2005). Hence, the overexpression of Cdc25B, as well as the alteration of the mechanisms that regulate the activity of Cdc25B can provoke a premature entry into mitosis contributing to neoplastic transformation (Sexl et al. 1999; Blomberg & Hoffmann 1999).

Cdc25C regulates the entry into mitosis. Cdc25C is predominantly a nuclear protein in mammalian cells. During the interphase, Cdc25C is inactive and it is localized in the cytoplasm through the association with 14-3-3 proteins. Cdc25C activity promotes the complete activation of Cdk1/cyclinB complex and regulates the G2 checkpoint allowing the entrance into mitosis. Cdc25C has several phosphorylation sites that are involved in its activation or inactivation. Polo like kinases (PLK) phosphorylates Cdc25C on Ser198 and induces its translocation to nucleus, promoting the progression of the cell cycle. Instead, during DNA damage, p53, Chk1 and Chk2 phosphorylate some serine residues of Cdc25C, arresting the cell cycle in the G2/M phase and preventing the transmission of the mutations to the daughter cells. The overexpression of Cdc25A and Cdc25B in various cancers is note, but little is known about the expression of Cdc25C in tumors and of its mechanism of action. However, it has recently been shown that this cell cycle regulator can

play an important role in clinical treatment as a potential target for a new generation of cancer therapy. Indeed, Cdc25C has been shown to be a novel tumor-associated antigen. Different studies have shown that in lung, gastric, bladder, prostate, esophageal squamous cell carcinoma, breast, acute myeloid leukemia, and colon cancers Cdc25C is more expressed than in normal tissues. Cdc25C has increased expression in squamous cell carcinoma and in particular, it has been found that hyperphosphorylation of Cdc25C Ser216 is closely related to tumorigenesis (Liu et al. 2020). Moreover, the overexpression of one splice variant of Cdc25C, i.e. Cdc25C1, respect to the other isoforms, appears to be correlated to the multidrug-resistance showed by some breast cancer cell lines (Albert et al. 2011).

Recent data suggest that the oncogenic role of Cdc25A, Cdc25B and Cdc25C may be also linked to their anti-apoptotic function. In particular, in non-melanoma skins cancers an increase of cytoplasmic levels of Cdc25 phosphatases represents a mechanism by which the tumor escapes from the apoptotic cell death. Indeed, some evidences suggest that the cytoplasmic localization of Cdc25 proteins, regulated by both post-translational modifications and protein-protein interactions, is closely linked to their alternative anti-apoptotic function (Al-Matouq et al. 2017; Liu et al. 2020).

As Cdc25 phosphatases are key cell cycle regulators and are overexpressed in different types of tumors, they represent an attractive target for new anticancer therapies. Many studies have been devoted to the synthesis and biochemical/biological characterization of molecules endowed with inhibitory activity towards Cdc25 phosphatases. To date, natural and synthetic molecules with inhibitor activity on Cdc25 enzymes have been discovered. The first inhibitors of Cdc25, identified in 1994, were the antitumor antibiotics DnacinA1 and B1, which were isolated from a strain of Actinobacteria (Horiguchi et al. 1994). Other compounds belong to different chemical classes, such as phosphate bioisosteres, electrophilic entities, peptide analogues and

quinone-based structures. In particular, analogues of Vitamin K and quinones represent the most studied Cdc25 inhibitors (Lazo & Wipf 2008). Regarding the inhibitory behaviour, there are three possible mechanisms through which these molecules can inhibit Cdc25s, i.e. reversible inhibition through binding to the active site of Cdc25, irreversible inhibition through a direct binding of inhibitor to Cdc25, or oxidation of the critical cysteine residue in the catalytic domain (HCX_5R) by reactive oxygen species (ROS) generated in cultured cells treated with quinone derivatives (Lazo et al. 2002; Kar et al. 2003; Zhou et al. 2009; Lavecchia et al. 2012; Capasso et al. 2015; Cerchia et al. 2019).

Some Cdc25s inhibitors are reported below:

- Indolylhydroxyquinone 8L is a compounds that display a reversible inhibition kinetic (Sohn et al. 2003).

- Compound LGH00031 is an irreversible inhibitor of Cdc25B, with IC50 values of 0.143-0.328 μM. It is able to inhibit the proliferation of several cancer cell lines (Zhou et al. 2009).

- NSC95397 is an anticancer drug that inhibits Cdc25B (Lazo et al. 2002).

- NSC119915 is an irreversible inhibitor of Cdc25A and Cdc25B. This compound affects the growth of various cancer cell lines and induce the arrest of the cell cycle in G0/G1 and G2/M phase (Lavecchia et al. 2012).

- IRC-083864 is a bis-quinonoid endowed with strong inhibitor activity, having an IC50 value of 20 nM (Brezak et al. 2009).

- CHEQ2 inhibits Cdc25A and Cdc25B and presents high tumor suppression properties inducing cell cycle arrest and apoptosis (Song et al. 2014).

However, despite the therapeutic potential of these compounds, many of the most potent Cdc25 inhibitors are strong oxidizing agents. It has been shown that these molecules, and in particular quinonoid compounds, induce a non-

tumor specific increase of the intracellular ROS levels that limits their application as anticancer drugs because of their toxic side effects. (Sur & Agrawal 2016). In some cases, the toxic side effect may be due to the nonspecific activity of ROS, produced by quinone-containing agents, that may oxidize other phosphatases or induce cell death also in non-tumor cells (Brisson et al. 2005; Cerchia et al. 2019). For this reason, a great part of compounds endowed with inhibitory potency toward Cdc25 enzymes have not entered clinical trials. Indeed, only a limited number of Cdc25 inhibitors produced an effect on tumor growth inhibition of xenografted human tumors in nude mice. In particular, BN82685 reduced tumors derived from pancreatic carcinoma cells (Brezak et al. 2005), IRC-083864 is active against prostatic and pancreatic tumors (Brezak et al. 2009), and PM-20 was successful in treating hepatoma tumors (Heidenreich et al. 2006) and polycystic kidney and liver disease in rodents (Masyuk. 2012).

1.3 Melanoma

Melanoma is one of the most aggressive and deadly tumors. The discovery of the most ancient melanoma cases date back to 2000 years ago, in Perú Inca mummies. However, melanoma was first formally described in 1804 by the physician Rene Laennec (Scolyer 2011). Nowadays, it is known that melanoma is a type of cancer that develops through malignant transformation of melanocytes, melanin-producing cells, resident in the basal layer of the epidermidis (Figure 3) (Lugović-Mihić 2019). Melanocytes have a neuronal origin because they give rise in the neural crest of the embryos and spread to different body districts, such as skin, mucous membrane, eyes, esophagus and meningeal coverings. Consequently, melanomas can arise in all sites mentioned above, but it is most frequent in the skin, in particular in the hair follicles. Moreover, it has been hypothesized that the neural origin of melanoma is responsible of its high invasiveness.

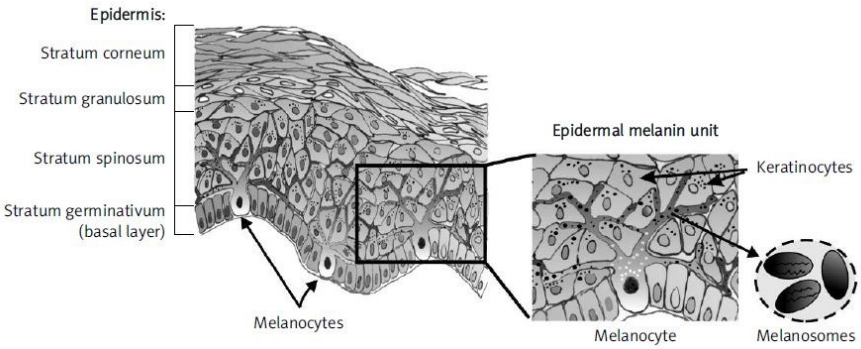

Figure 3. Scheme of the epidermis structure. Melanocytes reside between the basal layer cells and through dendritic processes communicate with about 30-40 keratinocytes in the epidermal melanin unit. Melanocytes synthesize melanin in melanosomes transported into keratinocytes to protect them from UV radiation (*Cichorek et al 2013*).

Although melanoma represents only 5% of skin cancer cases, it provokes the largest part of all skin cancer death, because of its peculiar invasive nature (Arozarena & Wellbrock 2017). Melanoma is characterized by a limitless growth, tissue invasion and metastasis that are sustained by growth factor independence, unresponsiveness to growth inhibitors and inhibition of apoptosis. It rapidly spreads due to infiltration of malignant cells into tissues, lymphatic and blood vessels. Its metastases are often localized in lymph nodes, brain, liver and other organs. Historically, melanomagenesis was conceived to occurs in a serial linear model, starting from benign nevi, then moving through 'intermediate' lesions, eventually leading to malignant tumors with metastatic potential. However, recent evidences suggest that not only are there multiple pathways by which a melanocyte may transform into a melanoma but also that some of the intermediate steps may be bypassed and that other non-linear biopathways exist. In particular, recent evidences indicate that aberrant mechanisms promote melanoma progression and metastasis, including the factors involved in the dysregulation of melanocyte proliferation, impairment of the immune system, and extrinsic agents in the tumor microenvironment that promote primary and metastatic growth (Jackett & Scolyer 2019).

As in other tumors, the pathogenic features of melanoma arise from genetic or epigenetic mutations that provoke the activation of specific oncogenes and/or inactivation of tumor-suppressor genes. However, both environmental and genetic factors concur to the onset of melanoma. The patients affected by melanoma often present a genetic predisposition, suppressed immune response, phenotypic features such as fair skin, blond or red hair, green or blue eyes and recurrent sunburns in their early lifetime. Indeed, the UV exposure and the subsequent skin burns play a key role in the melanoma development (Lugović-Mihić 2019).

The first classification of melanoma goes up to ’60 years of last century by work of Wallace Clark, Vincent McGovern, Martin Mihm, Richard Reed, but during the last decades new morphological and molecular features were found in different types of melanomas (Scolyer 2011).

The melanomas can be classified in four subtypes according on the tissues from which the primary tumors arise:

- Cutaneous melanoma (CM) that origins from non-glabrous skin. It is the most common subtype and is strongly related to skin UV exposure. It is more common in European descendents.
- Acral melanoma (AM) that arises in glabrous skin. Typically rise up on palms, soles and nail beds and occurs manly in African, Asian and Latin American descendents.
- Mucosal melanoma (MM) that develops from mucosae of the inner organs. This is the rarest one and is characterized by a particularly aggressive clinical course.
- Uveal melanoma occurs in the uvea of the eye.

A further classification of cutaneous melanoma is based on the occurrence of driver mutations (Rabbie et. Al 2018):

- BRAF-mutant
- N-H-KRAS-mutant
- NF1-loss
- triple wild-type (TWT)

Mutations in BRAF and NRAS encoding genes are most commonly detected in primary cutaneous melanomas. The most frequent gene mutated in melanomas is BRAF (50%), which encodes for the serine/threonine-protein kinase B-Raf, a protein kinase involved in the transduction of mitogenic signals, in particular in the MAPK (mitogen-activated protein kinase cascade) signal transduction pathway. The MAPK signal pathway controls the cellular proliferation, growth, and migration. The MAPK pathway starts with the binding of a growth factor to a tyrosine kinase receptor that activates the RAS kinases and ends with the activation of ERK, a serine threonine kinase capable to promote the expression of specific genes correlated with the cellular growth, proliferation and migration. Nearly 80-90% of benign and dysplastic nevi present a BRAF mutation for the amino acid residue valine 600. Moreover, it has been observed that the BRAF V600 mutation represents one of the first steps during melanoma development. In particular, 70% of BRAF mutations consist in the replacement of thymine with adenine leading to the placement of glutamate instead of valine at 600th amino acidic residue position (V600E). This mutation induces the constitutive activation of B-Raf, which leads to an excessive amplification of the cellular growth signals. In 20% of melanomas there were found mutations that activate N-Ras. N-Ras activating mutations induce the activation of two signalling pathways, MAPK and PI3K-AKT-mTOR. The PI3K-AKT-mTOR intracellular signalling pathway regulates the progression of cell cycle, because it is related to cell proliferation and potentially to cancer development. Other mutations can activate this pathway such as those involving NF1 that lead to a loss of c-KIT or PTEN expression or

overexpression of c-MET (Lugović-Mihić 2019, Tsao et. al 2003). Activating N-Ras and B-Raf mutations followed by ERK-mediated proliferation and survival are generally essential but not sufficient to melanoma growth. Combinations of these mutations with other genetic modifications create prerequisites for melanoma development.

However, the constitutive activation of BRAF in melanoma has a so crucial role in the tumor progression that it becomes a therapeutic target. The knowledge acquired on the molecular mechanisms that govern the melanomagenesis have permit to develop a variety of drugs targeting molecules involved in this process. Indeed, targeted therapy of melanoma includes B-Raf inhibitors, such as vemurafenib, dabrafenib and encorafenib that impair the transduction of signals, hinder cellular proliferation and reduce tumor growth. Unfortunately, almost all patients develop resistance to targeted therapy usually in the first 12 months of treatment (Kuske et al. 2018). This can be due to the activation of compensative survival mechanisms, such as the Akt pathway, inducing the selection of B-Raf inhibitors resistant melanoma cells with consequent increase of invasion and metastatic features (Arozarena and Wellbrock 2017). Immunotherapy is an alternative treatment modality that harnesses the power of the host's adaptive immune system by enhancing its own immune surveillance capabilities. In particular, the immunotherapy consists in the use of human antibodies that target immune checkpoint receptors, such as CTLA-4 and PD-1. These receptors exert a suppressive action on the immune response. The immunotherapeutic drugs, like ipilimumab or nivolumab, disable the suppression of the immune response and hence allow the T-cell activation. This therapy has translated into significant clinical outcomes with pathological regression and improved survival occurring in 30-40% of advanced melanoma patients. However, resistance to immune therapies inevitably develops. The treatments of metastatic and early-stage melanoma includes also the combination of immunotherapy and targeted therapies, that extended the overall survival (OS) of patients up to 36 months. In the patients

with BRAF mutations, the action of this therapy is rapid, and completely controls the proliferation and the survival of melanoma cells. B-Raf inhibitors revert the immune escape mechanisms put in place by melanoma cells, inducing an antitumor immunity response. Hence, treatment with B-Raf inhibitors improves the production of melanoma antigens, supporting the T-cell activity (Ruocco et al. 2019; Rabbie at al. 2018). However, the combination of immunotherapy with targeted therapy may improve the response but may be associated with unacceptable toxicity (Rabbie at al. 2018; Ruocco et al. 2019; Jackett & Scolyer 2019).

In recent years, the treatment of patients with metastatic melanoma has positively changed and several options are now available, especially for patients with the BRAF mutations. Immunotherapy and targeted therapy became the new standard of treatment. These advances have substantially improved survival rates. However, many questions still remain unanswered, such as what is the best first- and second-line treatment and the best treatment sequence. New combinations of drugs, targeted therapy combined with immunotherapy and sequencing approaches, are now underway in many clinical trials. Moreover, a personalized approach based on the identification of biomarkers could help in the choice of a better treatment (Vanella et al. 2019).

2. AIM OF THE RESEARCH

Cdc25 phosphatases are key enzymes in the regulation of cell cycle progression (Kristjànsdòttir & Rudolph 2004). Hence, dysregulation of Cdc25s can contribute to genomic instability that finally can lead to pathological conditions, including cancer. Indeed, Cdc25s have been found overexpressed in many cancers and often associated with more aggressive tumors and poor clinical outcome (Sur & Agrawal 2016). Therefore, Cdc25s can be considered potential targets for anti-cancer therapies. Many natural and synthetic molecules have been identified as inhibitors of Cdc25 enzymes (Tao et al. 2020) and most of them are characterized by a quinonoid structure. However, to date, a great part of compounds endowed with inhibitory potency toward Cdc25 enzymes have not entered clinical trials because of their possible side-toxic effects (Brisson et al. 2005; Evain-Bana et al. 2017). Previous studies, conducted in my research group, have identified the compound **NSC28620**, a non-quinonoid molecule, as an inhibitor of Cdc25 enzymes (Lavecchia et al. 2012). Non-quinonoid molecules are particularly attractive because they are intrinsically endowed with lower side-toxic effects. Hence, the aim of my research has been the biochemical characterization as well as the evaluation of the biological effects of 31 derivatives, designed from the lead compound **NSC28620**. In particular, the inhibition potency and the mechanism of action these molecules were investigated. Furthermore, biological studies have been conducted to evaluate the potential toxicity of these novel inhibitors in melanoma cell lines. It is known that melanoma is the most aggressive skin tumours and can be refractory to anti-cancer therapies. Hence, the discovery and characterization of new molecules acting through the modulation and inhibition of key pathways involved in cell proliferation and survival will be very helpful in the development of new therapeutic strategies against melanoma.

3. MATERIALS AND METHODS

3.1 Materials and reagents

The **NSC28620** derivatives, purchased from the Department of Pharmacy, University of Naples Federico II, were prepared as stock solutions in dimethylsulfoxide (DMSO) at 20 mM concentration; when diluted in the aqueous solution, the final concentration of the various compounds never exceeded 50 μM. The stock solution of 3-O-methylfluorescein phosphate (OMFP) was prepared in methanol at 2 mM concentration. The recombinant forms of Cdc25A, -B, and -C catalytic domain were obtained by means a heterologous expression system constituted by the vectors pET28a-Cdc25A-cd, pET28a-Cdc25B-cd, or pET28a-Cdc25C-cd, kindly provided by H. Bhattacharjee (Florida International University, Herbert Wertheim College of Medicine, Miami, Florida) and the Escherichia coli BL21(DE3) strain from Novagen. In the preparation of the recombinant enzyme, the buffers used for the purification procedure and storage were slightly modified by thoroughly replacing 10 mM β-mercaptoethanol as a reducing agent with 0.5 mM tris-(2-carboxyethyl)-phosphine hydrochloride (TCEP) (Bhattacharjee et al. 2010). The phosphate-buffered saline (PBS) contains 10 mM Na_2HPO_4, 2 mM KH_2PO_4, pH 7.4, supplemented with 137 mM NaCl and 2.7 mM KCl. Dulbecco's modified Eagle's medium (DMEM), Medium 199, fetal bovine serum (FBS), L-glutamine, penicillin G, streptomycin, and trypsin were purchased from Lonza (Milano, Italy). Isopropyl-β-thiogalactopyranoside (IPTG), TCEP, OMFP, propidium iodide (PI), crystal violet were purchased from Sigma Aldrich. The inhibitor of protease cocktail was obtained from Roche Diagnostics. Caspase-3 and caspase-9 activity fluorimetric assay kits were purchased from BioVision (Milpitas, CA, USA). The pan-caspase inhibitor Z-VAD-FMK was purchased from Selleckchem (USA). Rabbit monoclonal antibody against GAPDH and rabbit polyclonal antibody against p-Cdk1 were purchased from Cell Signaling Technology (Boston, USA).

Mouse monoclonal antibody against COX-IV was purchased from Elabscience (Houston, USA). Mouse monoclonal antibody against β-tubulin was purchased from Sigma-Aldrich (Darmstadt, Germany). FITC donkey, anti-mouse secondary antibody was purchased from Jakson ImmunoResearch (Suffolk,UK). Rabbit polyclonal antibodies against β-actin, Cdc25B, pAkt (Ser473) or Akt and mouse monoclonal antibodies against cytochrome *c*, Cdc25A, Cdc25C or p53, and the HRP conjugated secondary antibody were purchased from Santa Cruz Biotechnology (Heidelberg, Germany). All other reagents and solvents of high analytical grade were purchased from Sigma-Aldrich.

3.2 Kinetic studies of the Cdc25 phosphatase activity

To measure the dephosphorylation of OMFP catalyzed by the recombinant Cdc25 forms was used a fluorimetric assay method (Capasso et al. 2015, Lavecchia et al. 2012). Brefly, the formation of the fluorescent product O-methylfluorescein (OMF) was monitored continuously at 30 °C by means the computer-assisted Cary Eclipse spectrofluorimeter (Varian) equipped with a thermostatic controller. The wavelength of excitation was set at 485 nm, whereas the emission wavelength was set at 530 nm, respectively. Both excitation and emission slits were set at 10 nm. The final volume of the reaction mixture was 500 μL. The reaction mixture, containing a fixed concentration of Cdc25A, -B, or -C ranging between 15 and 25 nM in 20 mM Tris-HCl, pH 7.8, 0.5 mM TCEP, was prepared in the absence or in the presence of various concentrations of each among 31 inhibitors. The reaction mixture also contained 1% (v/v) DMSO carried over from the inhibitors. After the addition of 0.5-25 μM OMFP, the velocity of OMFP hydrolysis (v_i) was measured and expressed as arbitrary units per min. The data of v_i were analyzed as a function of [OMFP] in double reciprocal Lineweaver-Burk plots, thus allowing the extrapolation of the values of affinity for the substrate OMFP (K_M) and the maximum velocity of OMFP hydrolysis (V_{max}). The comparison

of the Lineweaver-Burk plot of phosphatase activity in the absence of inhibitor with those obtained in the presence of different concentrations of the inhibitor allowed the calculation of the inhibition constant (K_i) of Cdc25 forms toward the various compounds. The K_i was calculated using the resulting values of K_M for OMFP and V_{max} in presence of the inhibitor according to the following equations. When the K_M remained essentially unchanged, but the V_{max} decreased after the addition of the inhibitor (noncompetitive inhibition), the K_i was calculated with the equation: $K_i = V_{max\ +I}\cdot[I]/(V_{max} - V_{max\ +I})$, where $V_{max\ +I}$ represents the V_{max} measured in the presence of the inhibitor (I). When both K_M and V_{max} underwent a similar and progressive decrease after the addition of the inhibitor (uncompetitive inhibition), the K_i could be calculated with either the former equation or an alternate equation: $K_i = K_{M+I}\cdot[I]/(K_M - K_{M+I})$, where K_{M+I} represents the K_M measured in the presence of the inhibitor. On the other hand, in the case of mixed inhibition, only a rough evaluation of the K_i value was possible based on the decrease of V_{max} and increase of K_M after the addition of the inhibitor.

3.3 Preparation of Cdc25B-C473S

To obtain the mutant form of Cdc25B that contains the C473S replacement (Cdc25B-C473S) a site-directed mutagenesis of the Cdc25B catalytic segment was performed and cloned in pET28a-Cdc25B-cd. In particular, the QuikChange site-directed mutagenesis kit (Stratagene, La Jolla, CA) and the specific forward and reverse primers for C473S replacement (5'd-ATCCTCATTTTCCACTCTGAATTCTCATCTGAG-3' and 5'd-CTCAGATGAGAATTCAGAGTGGAAAATGAGGAT-3'), were used. The nucleotide sequencing of the mutagenized segment of the positive clones excluded the presence of undesired mutations. The new vector was called pET28a-Cdc25B-C473S-cd. The expression of the new vector and the purification of the recombinant form of Cdc25B-C473S catalytic domain was carried out as previously reported for wild-type Cdc25B catalytic domain

(Cerchia et al. 2019), and similar yields were obtained. As expected, the mutant enzyme was unable to hydrolyse the synthetic substrate OMFP, when its activity was checked with the fluorimetric assay method.

3.4 Fluorescence studies on the purified catalytic domain of Cdc25B and Cdc25B-C473S

Fluorescence spectra were recorded at 20°C using a computer-assisted Cary Eclipse spectrofluorimeter (Varian) equipped with a thermostatic controller. The excitation wavelength was set at 280 nm and the excitation and emission slits were set at 10 and 20 nm, respectively. The 0.2 μM solution of Cdc25B or Cdc25B-C473S dissolved in 500 μL final volume of 20 mM Tris•HCl, pH 7.8, 0.5 mM TCEP was directly prepared in the fluorimetric cuvette in the absence or in the presence of OMFP and/or some **NSC28620** derivatives. Serial pre-dilutions of the derivatives or OMFP at increasing concentration were prepared in DMSO or methanol, respectively. Alongside, convenient amount of a pre-dilution of the enzyme was prepared just before its usage for the experiment and stored on ice. When the combined effect of derivative and OMFP was investigated, two enzyme pre-dilutions were prepared in the absence or in the presence of 5 μM OMFP. In order to evaluate the specific effect produced by any addition of solvent/ligand on the intrinsic fluorescence of the enzyme, 495 μL of the enzyme pre-dilution were placed in the fluorimetric cuvette and the relative spectrum was recorded; after the addition of 5 μL of each pre-dilution of solvent/ligand and fast mixing, the spectrum was recorded again. This procedure, repeated for each experimental point, allowed a normalization of the specific effects produced by solvent/ligands. Moreover, a correction was also applied for the little inner-filter effect due to the absorbance at 280 nm of the derivative used at different concentrations; on the other hand, no correction was necessary for OMFP. All spectra, recorded at a scan speed of 120 nm/min, were normalized and corrected.

3.5 Cell cultures

The human melanoma cell lines A375 (deriving from a primary tumor) and A2058 (deriving from lymph nodal metastasis) were kindly provided from CEINGE (Naples, Italy). Cells were cultured in humidified incubator at 37 °C under 5% CO_2 atmosphere and grown in DMEM supplemented with 10% FBS, 2 mM L-glutamine, 100 IU/mL penicillin G and 100 μg/mL streptomycin. The human skin fibroblast cell line BJ-5ta, immortalized with the human telomerase reverse transcriptase (Albano et al. 2013), was cultured in a 4:1 mixture of DMEM and Medium 199 supplemented with 4 mM L-glutamine, 4.5 g/L glucose, 1.5 g/L sodium bicarbonate, 10% FBS, 100 IU/mL penicillin G, 100 mg/mL streptomycin in humidified incubator at 37 °C under 5% CO_2 atmosphere. All cells were split and seeded every 3 days and used during their exponential phase of growth. Cell treatments were usually carried out after 24 h from plating.

3.6 MTT assay

The 3-(4,5-dimethylthiazol-2-yl)-2,5-biphenyltetrazolium bromide (MTT) assay was used to detect cell viability essentially as previously described (Gelzo et al. 2014). Briefly, A2058 cells were plated in 96-well microtiter plates at 4×10^4 cells/well. After 24 h, cells were treated with different concentrations of the various inhibitors or with 0.5% (v/v) DMSO as a control vehicle. After 24, 48, or 72-h treatment and upon addition of 10 μL MTT solution in the dark, plates were incubated for 3 h at 37 °C under 5% CO_2 atmosphere. After medium aspiration and solubilization of formazan crystals, the absorbance was measured at a wavelength of 570 nm using an ELISA plate reader (Bio-Rad, Milano, Italy).

3.7 Colony formation assay

Colony-forming assay was performed as previously described with some modifications (Rafehi et al. 2011). Briefly, cells were seeded at a density of 4 ×

10^2 cells/well in 6-wells plates, in duplicate. After 2/3 days, cells were treated with different concentrations of the compound **4a** or 0.5% (v/v) DMSO as control vehicle and the incubation was prolonged for further 10 days at 37 °C under 5% CO_2 atmosphere. Then, colonies were stained with 1% (w/v) crystal violet in 50% (v/v) ethanol for 1 h at room temperature. Cells were photographed with a digital camera (Canon PowerShot G9); the number of colonies (≥50 cells per colony) was counted using ImageJ 1.42q software.

3.8 Cell cycle analysis

Cells were pleated at 3×10^5 cells/well into 6-well plates. After 24 h, cells were treated with 10 μM **4a** or 0.5% (v/v) DMSO and incubated at 37 °C for 8 or 16 h. At the end of each treatment, cells were harvested with trypsin, centrifuged, and the pellet was resuspended in PBS. Cells were fixed with 70% (v/v) cold ethanol and stored at −20 °C for 1 h. Then, cells were washed with cold PBS and centrifuged. The pellet was resuspended in 200 μL of a non-lysis solution containing 50 μg/mL PI and incubated at 4 °C for 30 min. To evaluate the distribution of cell cycle phases, the cells were analyzed with a FACScan flow cytometer (Becton Dickinson).

3.9 Analysis of apoptosis

The number of apoptotic nuclei was detected through cytofluorimetric analysis. Briefly, cells were seeded into 6-well plates at 3×10^5 cells/well and after 24 h were treated with **4a** or 0.5% (v/v) DMSO and incubated for different times. Then, cells were harvested with trypsin, centrifuged, and the pellet was resuspended in 200 μL of a hypotonic lysis solution (0.1% (w/v) sodium citrate, 0.1% (v/v) Triton X-100, and 50 μg/mL propidium iodide) containing PI. After incubation at 4°C for 30 min, cells were analyzed with a FACScan flow cytometer (Becton Dickinson) to evaluate the presence of nuclei with DNA content lower than diploid.

3.10 Measurements of caspase-9 and caspase-3 activity

The enzymatic activity of caspase-3 and caspase-9 was measured by using caspase-3 and -9 fluorimetric assay kits, respectively, according to the manufacturer's protocol. Briefly, cells were seeded into 75 cm^2 plates at the density of 2×10^6 cells/plate. After 24 h the cells were treated with **4a** or 0.5% (v/v) DMSO for 24 h. After the treatment, cells were collected, washed with PBS and finally lysed at 4 °C in the cell lysis buffer. The cell lysates were incubated at 37° C for 2 h with 50 μM LEHD-AFC or DEVD-AFC substrates to measure the caspase-9 or caspase-3 activity, respectively, using a Cary Eclipse spectrofluorimeter (Varian). The excitation wavelength was set at 400 nm and emission at 505 nm. Both excitation and emission slits were set at 10 nm.

3.11 Total cell lysates and subcellular fractionation for western blotting analysis

To obtain the total protein extract, cells were seeded into 6-well-plates (3×10^5 cells/plate) for 24 h at 37 °C and then treated with **4a** or 0.5% (v/v) DMSO. After treatments, cells were harvested, washed with PBS, and then lysed in ice-cold modified radio immunoprecipitation assay (RIPA) buffer (50 mM Tris-HCl, pH 7.4, 150 mM NaCl, 1% Nonidet P-40, 0.25% sodium deoxycholate, 1 mM Na_3VO_4 and 1 mM NaF), supplemented with protease inhibitors and incubated for 30 min on ice. The supernatant, containing the total protein extract, was obtained after centrifugation at 13200 g for 30 min at 4 °C. Protein concentration was determined by the Bradford method, using bovine serum albumin (BSA) as standard (Bradford 1976). In order to obtain the cytosolic and mitochondrial fractions, cells were plated at a density of 2×10^6 cells/plate for 24 h at 37 °C. After treatment with **4a** or 0.5% (v/v) DMSO, cells were harvested, washed in PBS, and then resuspended in buffer A (5 mM Hepes, pH 7.4, 250 mM mannitol, 0.5 mM EGTA, 0.1% BSA), supplemented with protease inhibitors, and homogenized. The homogenate was centrifuged at 600

g for 5 min at 4 °C and the supernatant was then centrifuged at 10300 g for 10 min at 4 °C. The resulting supernatant represented the cytosolic fraction, whereas the pellet, constituting the mitochondrial fraction, was resuspended in RIPA buffer. Protein concentration was determined as indicated above. Equal amounts of total, cytosolic or mitochondrial protein extracts were used for Western blotting analysis. Briefly, protein samples were dissolved in SDS-reducing loading buffer, run on sodium dodecylsulfate polyacrylamide gel electrophoresis (SDS/PAGE), and then transferred to Immobilon P membrane (Millipore). The filter was incubated with the specific primary antibody at 4 °C overnight and then with the secondary antibody at room temperature for 1 h. Membranes were then analyzed by an enhanced chemiluminescence reaction using WesternBright ECL (Advansta) according to manufacturer's instructions; signals were visualized by autoradiography. The analysis of pAkt protein levels was performed as previously described (Arcucci et al. 2014). Briefly, the filters were first incubated with the anti-pAkt primary antibody and then with the secondary antibody and membranes were analysed by an enhanced chemiluminescence reaction as previously indicated. Before the incubation with the another primary antibody, the same filters were stripped, using AbCam stripping solution, pH 2 (200 mM glycine, 3.5 mM SDS, 1% Tween-20) at 45 °C for 30 min, washed 3 times with PBS-Tween 0.1%. The filters were incubated with anti-Akt primary antibody and then with the relative secondary antibody. Signals were detected as previously described.

3.12 Immunofluorescence staining

Immunofluorescence experiments were carried out essentially as previously described (Arcucci et al. 2011). Briefly, cells were plated on glass coverslips at a density of $3x10^5$ cells/well in 6-well plates, and after 24 h were treated with **4a** or 0.5% (v/v) DMSO. At the end of treatment, cells were incubated with 90 nM MitoTracker Red (Invitrogen, Inchinnan, UK) at 37 °C for 1 h and then washed three times with ice-cold PBS. Cells were fixed with 4%

paraformaldehyde, and then blocked in donkey serum (Millipore) diluted 1:10 in PBS, for 30 min at room temperature. Glass coverslips were incubated for 1 h at 37 °C with a mouse monoclonal antibody against cytochrome *c*, diluted 1:50 in PBS, washed three times with PBS and subsequently incubated for 1 h at 37 °C with a FITC donkey anti-mouse secondary antibody diluted 1:50 in PBS. After three washings in PBS, the cell nuclei were labelled with DAPI (Vector Laboratories, Inc., Burlingame, CA, USA). Glass coverslips mounting was done in Vectashield (Vector Laboratories). The images were taken with digital camera connected to the microscope (Leica DFC345FX, Leica Microsystems, Wetzlar, Germany) and then merged with the software Leica Application Suite 3.6.

3.13 Statistical analysis

Data are reported as the mean ± standard error (SE). The statistical significance of differences among groups was evaluated using ANOVA, with the Bonferroni correction as post hoc test or the Student t-test where appropriate. The significance was accepted at the level of $p < 0.05$.

4. RESULTS

4.1 Optimization program of the lead compound NSC28620 to target the Cdc25B phosphatase

In a previous work it was demonstrated that the non-quinone compound **NSC28620**, identified by a structure-based virtual screening method, acted as a reversible inhibitor of Cdc25B with a K_i value of 5.3 μM and affected the cell viability of some cancer cell lines (Lavecchia et al. 2012). To identify more potent Cdc25 inhibitors, possibly functioning as novel anticancer drugs, a lead optimization program on this promising inhibitor was undertaken and 31 novel molecules were synthesized in collaboration with the Department of Pharmacy, University of Naples Federico II. Based on the binding mode of **NSC28620** (Figure 4A), the designed structural modifications regarded four specific regions of the lead compound (Figure 4B) in order to improve its inhibition power. The changes were made to explore new potential hydrophobic and/or hydrophilic interactions with the catalytic site and/or the adjacent region, called swimming pool. As first, in all 31 derivatives the phthalic moiety of **NSC28620** was replaced by a bulkier naphthalene ring system, thus eliminating two out of three carboxylic groups of **NSC28620**. This novel system was undecorated (compounds 1-7) or decorated with hydroxy, methoxy, or amino groups linked to one of the positions 3, 4, and 5, corresponding to substituents R^1, R^2, and R^3, respectively (compounds 1a-c, 3a, 3b, 4a, 4b, 6a, 6b, 6d, 6e, 6f, 7a, 7b, 7d, 7e, 7f, 7i, 7j, 8, 9, 10, 11, and 12; Table 1). Another region target of the structural modifications regarded the remaining carboxyl group of **NSC28620**. In particular, this function was replaced at position 2 or 3 of the benzoyl moiety (substituents R^4 and R^5, respectively in compounds 1, 1a-c, 6, 6a, 6b, 6d, 6e, 6f, 7, 7a, 7b, 7d, 7e, 7f, 7i, 7j, and 12). Furthermore, in order to enhance the membrane permeability and ameliorate the cell uptake of the novel inhibitors, the carboxylic moiety was esterified in some compounds (2, 3a, 3b, 4, 4a, 4b, 8, 9, 10, and 11). Finally,

the carbonyl group (position X), that accepts a H-bond from Y428 OH group (Figure 4A), was replaced by an amino group in some derivatives, in order to explore the H-bond acceptor or donor capability at this position (compounds 3, 3a, 3b, 4, 4a, 4b, 5, 6, 6a, 6b, 6d, 6e, 6f, 7, 7a, 7b, 7d, 7e, 7f, 7i, 7j, 8, 9, 10, 11, and 12). Based on the identity at X position, the **NSC28620** analogs were grouped in naphthylphenylketone (NPK) or naphthylphenylamine (NPA) derivatives.

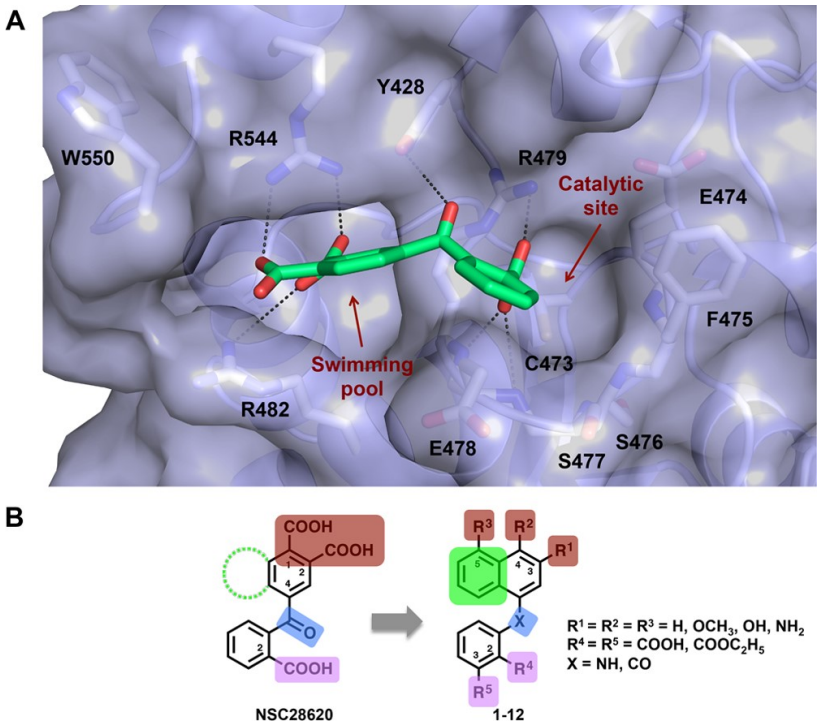

Figure 4. Structure-based optimization of lead NSC28620. (**A**) Predicted binding mode of **NSC28620** (green) in the Cdc25B binding cavity. For clarity, only interacting residues are displayed and labeled. Ligand and interacting key residues (white) are represented as stick models, while the protein is a transparent Connolly surface model. H-bonds and salt bridges are shown as dashed black lines. (**B**) Schematic overview of the rationally designed **NSC28620** derivatives.

Table 1. Structure and inhibition properties of thirty-one NSC28620 derivatives

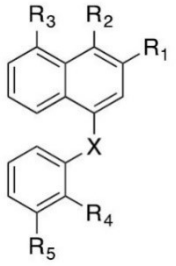

Cpd	R^1	R^2	R^3	R^4	R^5	X	K_i[a] (μM)	putative inhibition mechanism
1	H	H	H	COOH	H	CO	69	mixed
1a	OCH_3	H	H	COOH	H	CO	36	mixed
1b	H	OCH_3	H	COOH	H	CO	7.1 ± 0.9	noncompetitive
1c	OH	H	H	COOH	H	CO	34 ± 3	noncompetitive
2	H	H	H	$COOC_2H_5$	H	CO	54	mixed
3	H	H	H	$COOC_2H_5$	H	NH	2.8 ± 0.7	uncompetitive
3a	OCH_3	H	H	$COOC_2H_5$	H	NH	12.5 ± 2.6	uncompetitive
3b	H	OCH_3	H	$COOC_2H_5$	H	NH	6.9 ± 2.0	noncompetitive
4	H	H	H	H	$COOC_2H_5$	NH	7.3 ± 0.6	uncompetitive
4a	OCH_3	H	H	H	$COOC_2H_5$	NH	8.5 ± 1.2	uncompetitive
4b	H	OCH_3	H	H	$COOC_2H_5$	NH	11.9 ± 4.2	noncompetitive
5	H	H	H	H	H	NH	32	mixed
6	H	H	H	COOH	H	NH	22 ± 3	uncompetitive
6a	OCH_3	H	H	COOH	H	NH	16.9 ± 0.3	noncompetitive
6b	H	OCH_3	H	COOH	H	NH	6.1 ± 0.7	uncompetitive
6d	OH	H	H	COOH	H	NH	5.1 ± 0.7	noncompetitive
6e	H	OH	H	COOH	H	NH	2.7 ± 1.1	noncompetitive
6f	H	H	OH	COOH	H	NH	13.4 ± 1.1	noncompetitive
7	H	H	H	H	COOH	NH	30	mixed
7a	OCH_3	H	H	H	COOH	NH	55 ± 7	uncompetitive
7b	H	OCH_3	H	H	COOH	NH	45 ± 3	uncompetitive
7d	OH	H	H	H	COOH	NH	5.8 ± 0.8	noncompetitive
7e	H	OH	H	H	COOH	NH	6.4 ± 0.8	uncompetitive
7f	H	H	OH	H	COOH	NH	2.9 ± 0.3	noncompetitive
7i[b]	H	NH_2	H	H	COOH	NH	1.4 ± 0.3	noncompetitive
7j[b]	H	H	NH_2	H	COOH	NH	0.8 ± 0.2	noncompetitive
8	H	H	OH	$COOC_2H_5$	H	NH	7.4 ± 2.2	noncompetitive
9	H	H	OH	H	$COOC_2H_5$	NH	4.9 ± 1.3	noncompetitive
10[b]	H	H	NH_2	$COOC_2H_5$	H	NH	9.9 ± 3.2	noncompetitive
11[b]	H	H	NH_2	H	$COOC_2H_5$	NH	36 ± 3	noncompetitive
12	H	H	NH_2	COOH	H	NH	6.5 ± 1.4	noncompetitive
NSC28620							5.3 ± 2.4	competitive

[a]The values of K_i, calculated as indicated in Materials and Methods, are an average from at least three independent experiments. The missing standard deviation for mixed inhibitors is due to the fact that the K_i value indicated is just a rough evaluation of the inhibition power.
[b]Compounds were tested as hydrochloride salts.

4.2 Inhibition properties of NSC28620 derivatives on the phosphatase activity of the purified recombinant form of Cdc25B

The inhibition properties exhibited by the **NSC28620** derivatives were evaluated through kinetic measurements of the phosphatase activity of the recombinant form of Cdc25B. In detail, the hydrolysis rate of the synthetic substrate 3-O-methylfluorescein phosphate (OMFP) triggered by Cdc25B was measured in the absence or in the presence of various inhibitor concentrations and at different substrate concentrations. The obtained data of initial velocity (v_i) were analyzed through Lineweaver-Burk plots, thus allowing also an insight on the inhibition mechanism of the novel derivatives. As shown in Table 2, the affinity for the substrate OMFP measured in the absence of inhibitor (K_M = 2.7 ± 0.2 μM) remained essentially unmodified in the presence of most derivatives, whereas it decreased or slightly increased in the presence of the others. Conversely, all derivatives provoked a reduction of the maximum velocity of OMFP hydrolysis respect to that measured in the absence of inhibitor (V_{max} = 323 ± 10 AU/min). This finding indicates that all novel molecules acted as Cdc25B inhibitors with a modulation of their inhibition power. Interestingly, some inhibitors seemed to possess a stronger inhibition power compared with that exhibited by the lead compound (Table 1). Furthermore, the reduction of V_{max}, common to all derivatives, suggests that none of them could be ranked as a competitive inhibitor, differently from what observed for **NSC28620** (Lavecchia et al., 2012).

Table 2. Kinetic parameters of the Cdc25B phosphatase activity in the presence of NSC28620 derivatives

Compound	Concentration added (μM)	K_M [a] (μM)	V_{max} [a] (AU/min)
1	**30**	**3.6**	**241**
1a	**30**	**4.5**	**200**
1b	**10**	**2.7**	**148**
1c	**30**	**3.3**	**164**
2	**15**	**2.6**	**253**
3	**3**	**1.4**	**149**
3a	**10**	**1.3**	**166**
3b	**5**	**1.8**	**130**
4	**10**	**1.4**	**130**
4a	**15**	**1.2**	**97**
4b	**15**	**2.3**	**112**
5	**30**	**4.5**	**178**
6	**30**	**1.5**	**126**
6a	**30**	**2.7**	**103**
6b	**20**	**0.9**	**67**
6d	**30**	**1.8**	**51**
6e	**10**	**2.4**	**53**
6f	**15**	**3.3**	**158**
7	**30**	**4.9**	**163**
7a	**30**	**1.3**	**199**
7b	**30**	**1.5**	**184**
7d	**10**	**2.6**	**127**
7e	**10**	**1.7**	**135**
7f	**5**	**3.0**	**130**
7i	**5**	**3.7**	**78**
7j	**1**	**2.1**	**165**
8	**10**	**4.5**	**139**
9	**5**	**3.0**	**100**
10	**6**	**2.5**	**205**
11	**15**	**2.5**	**218**
12	**8**	**2.0**	**84**

[a] Kinetic parameters of the Cdc25B phosphatase activity in the absence of inhibitor: K_M for OMFP = 2.7 ± 0.2 μM; V_{max} = 323 ± 10 AU/min.

An inspection of the kinetic data in Lineweaver-Burk plots allowed a putative assignment of the compounds to different categories of inhibition mechanism. Hence, the novel inhibitors were classified as noncompetitive, uncompetitive, or mixed on the basis of the comparison of the Lineweaver-Burk plots obtained in the presence of different inhibitor concentrations with that obtained in the absence of inhibitor. For instance, as depicted in Figure 5A, **7j** appears as a typical noncompetitive inhibitor because the progressive decrease of the V_{max} at increasing inhibitor concentration occurs without a significant change of the K_M for OMFP (see also Table 2). On the other hand, **3** exhibits a kinetic behaviour approaching that of an uncompetitive inhibitor because the progressive decrease of V_{max} appears to be concomitant to a roughly similar

decrease of the K_M (Figure 5B and Table 2). This kinetic approach allowed the calculation of the inhibition constant (K_i) for each derivative on the basis of their effects on the kinetic parameters of the phosphatase reaction (Table 1).

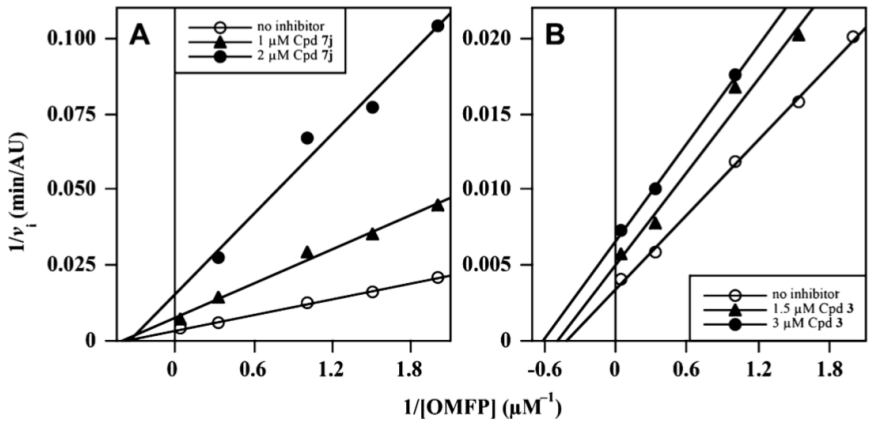

Figure 5. Effect of compound 7j or 3 on the Lineweaver-Burk plots of the Cdc25B phosphatase activity. The activity, measured through the OMFP hydrolysis rate as described in Materials and Methods, was determined in the absence (open circles in both panels) or in the presence of 1.0 μM or 2.0 μM compound **7j** (filled triangles or filled circles, respectively; panel (A) or 1.5 or 3.0 μM compound **3** (filled triangles or filled circles, respectively; panel (B).

The calculated K_i values range in the interval from 0.8 μM to 69 μM. In particular, some derivatives (**7j**, **7i**, **6e**, **7f**, or **3**) are endowed with a significantly stronger inhibition potency compared to that of the initial lead **NSC28620** (K_i = 5.3 μM), whereas the remaining compounds display a comparable or lower inhibition. The majority of the Cdc25B inhibitors are also active against Cdc25A and Cdc25C (Capasso et al. 2015; Lavecchia et al. 2012; Tao et al. 2020). Therefore, an inspection of the inhibition properties of some representative derivatives toward the recombinant forms of both Cdc25A and Cdc25C was performed. In particular, the K_i of **7j** toward Cdc25A and -C was 0.6 and 4.0 μM, whereas the corresponding values for **3** were 0.6 and 0.4 μM, respectively. This finding allows the speculation that the **NSC28620** analogues could be active also on Cdc25A and -C.

4.3 Intrinsic fluorescence of Cdc25B

A powerful strategy for studying the interaction between Cdc25B and its ligands (substrate and/or inhibitors) could be represented by the intrinsic fluorescence of the enzyme. Under this concern, the catalytic domain of Cdc25B contains a single tryptophan residue, W550, besides 11 tyrosines. In particular, W550 is located in the protein region called "swimming pool" for the presence of water molecules found in the crystal structure (Reynolds et al. 1999). The Figure 6 shows the emission spectrum of the recombinant form of Cdc25B; the positioning of the emission maximum at 357 nm, mainly due to the intrinsic fluorescence of tryptophan, indicates that this residue is exposed to solvent.

One of the Cdc25B ligands is OMFP, the common synthetic substrate used to measure the phosphatase activity of all Cdc25 forms. Upon its binding to the enzyme, the nonfluorescent OMFP is hydrolysed to the fluorescent product OMF (λ_{emis} = 530 nm) and this allows the measurement of the catalytic activity through the rate of OMF formation. In order to study the interaction between Cdc25B and OMFP without the "complication" of its hydrolysis, a recombinant mutant Cdc25B with the catalytic C473 residue replaced by serine was designed and prepared (Cdc25B-C473S). As supposed, this mutant form was unable to hydrolyze OMFP, thus allowing to record the intrinsic fluorescence of the enzyme without the interference of the fluorescent product OMF (data not shown). As shown in Figure 6, the emission spectrum of Cdc25B-C473S was almost superimposable to that of the wild-type recombinant Cdc25B. Hence, the C473S replacement caused the loss of catalytic activity, but did not alter the fluorescence emission of the enzyme. Therefore, we took advantage of these properties to study the interaction between the enzyme and substrate in the absence of catalysis.

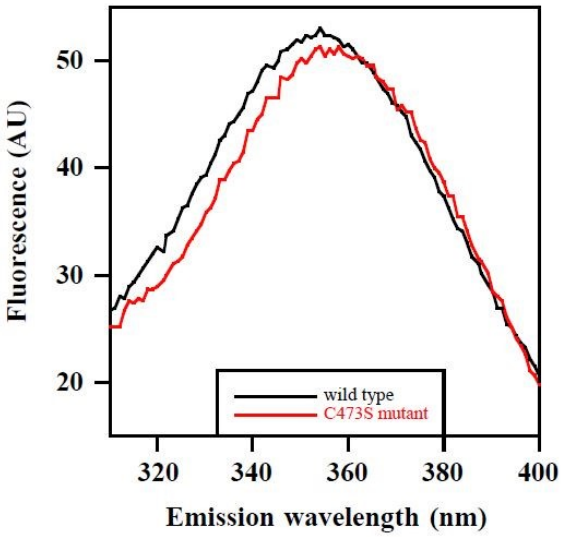

Figure 6. Intrinsic fluorescence of recombinant Cdc25B and Cdc25B-C473S. The fluorescence spectra of 0.2 µM Cdc25B (black line) or 0.2 µM CDC25B-C473S (red line) were recorded as indicated in Materials and Methods.

4.4 Interaction between Cdc25B-C473S and OMFP evaluated trough intrinsic fluorescence studies

The spectra of Cdc25B-C473S recorded in the presence of increasing OMFP concentration showed a clear dose-dependent quenching of the fluorescence yield, without a shift of the emission maximum (Figure 7A). The data obtained were analyzed through the Stern-Volmer equation, $F_0/Fs = 1 + K_{SV}$ [Q], allowing the study of the fluorescence quenching as a function of the quencher Q, where K_{SV} represents the Stern-Volmer constant for the formation of the binary complex Cdc25B•ligand. Thus, we compared the fluorescence emission at 357 nm recorded at each substrate concentration (F_S) with the corresponding value obtained in absence of substrate (F_0). The reduction of fluorescence linearly increased with [Q]. Indeed, the data fit a straight line starting from $F_0/Fs = 1$ with a slope corresponding to the K_{SV} value of 0.814 μM^{-1} (Figure 7B). The reciprocal of this value, i.e. 1.23 µM, represents the substrate

concentration leading to 50% quenching of Cdc25B-C473S fluorescence emission. This value could also correspond to the equilibrium dissociation constant (K'_D) of the enzyme•substrate complex. Interestingly, this value is even lower than the affinity constant K_M of the wild type Cdc25B for the substrate OMFP (K_M = 2.7 ± 0.2 µM). Therefore, these data suggest that Cdc25B-C473S tightly binds the substrate in a way similar to that of Cdc25B.

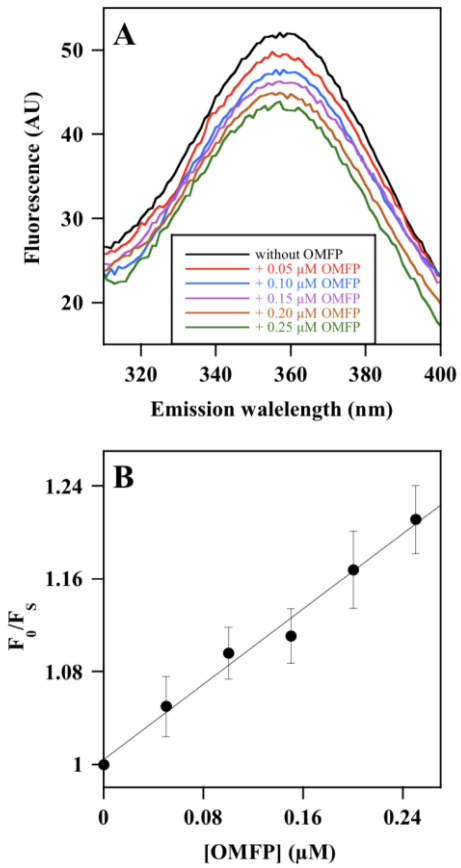

Figure 7. Effect of OMFP on the intrinsic fluorescence of recombinant Cdc25B-C473S. (A) The fluorescence spectra of 0.2 µM Cdc25B-C473S in the absence or in the presence of the indicated OMFP concentration were recorded and normalised as indicated in Materials and Methods. An identical 1% (v/v) final concentration of both methanol and DMSO is present in all samples. (B) The data of fluorescence emission at 357 nm obtained in the absence (F_0) or in the presence of each OMFP concentration (F_S) were treated according to the Stern-Volmer equation.

4.5 Interaction between Cdc25B and some NSC28620 derivatives evaluated through intrinsic fluorescence studies

The putative inhibition mechanism assigned to each **NSC28620** derivative through the Lineweaver-Burk plots (Table 1) was further investigated. Among the various derivatives, compounds **7j**, **7i** and **6e** were representative members of noncompetitive inhibitors, with K_i values of 0.8 μM, 1.4 μM and 2.7 μM, respectively. The emission spectra of intrinsic fluorescence of recombinant Cdc25B shown in Figure 8A→C indicate an evident dose-dependent quenching of fluorescence yield caused by each selected noncompetitive inhibitor, with some differences probably due to the relative inhibition power. As no shift of the emission maximum was observed, the fluorescence signal at 357 nm at each inhibitor concentration (F_I) was compared with the corresponding value obtained in the absence of inhibitor (F_0), using the Stern–Volmer equation. The plots of **7j**, **7i** and **6e** (Figure 8D→F) were used to calculate the K_{SV} values (0.129 μM^{-1} for **7j**, 0.069 μM^{-1} for **7i** and 0.035 μM^{-1} for **6e**). The reciprocal of these values (7.8 μM for **7j**, 14.5 μM for **7i** and 28.6 μM for **6e**) represents the inhibitor concentration leading to 50% quenching of Cdc25B emission and possibly evaluates the K'_D of the complex between Cdc25B and these typical noncompetitive inhibitors.

Compounds **3**, **4** and **4a**, with K_i values of 2.8 μM, 7.3 μM and 8.5 μM, respectively, were selected as representative members of putative uncompetitive inhibitors. Figure 9 shows that the intrinsic fluorescence of Cdc25B is only minimally affected by these inhibitors. Indeed, differently from the effects exerted by noncompetitive inhibitors, compounds **3**, **4** and **4a** (Figure 9A→C) exert a very low dose-dependent quenching of fluorescence. Indeed, when the data were analysed with the Stern-Volmer equation (Figure 9D→F), the calculated values of K_{SV} (0.011 μM^{-1} for **3**, 0.016 μM^{-1} for **4**, and 0.010 μM^{-1} for **4a**) were significantly lower than those obtained with the noncompetitive inhibitors. Hence, the inhibitor concentration leading to 50 %

quenching of Cdc25B emission is consistently greater than 50 µM for these inhibitors, a finding indicating that these compounds only display a very weak interaction with Cdc25B, at least in the absence of OMFP.

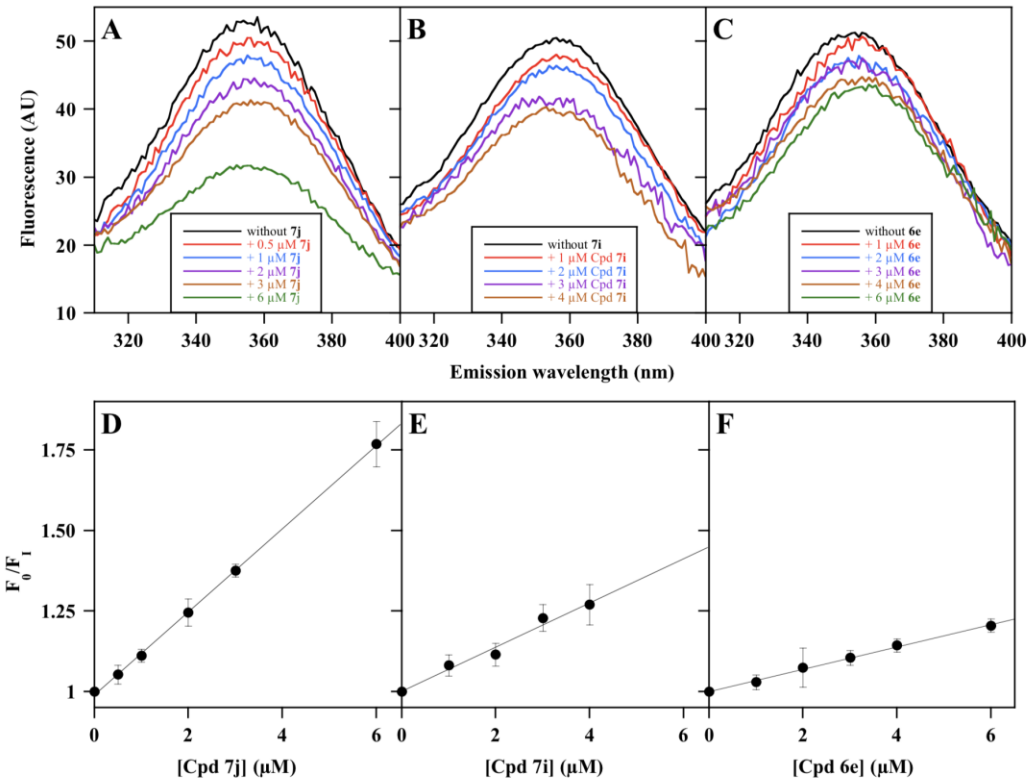

Figure 8. Effect of some noncompetitive inhibitors on the intrinsic fluorescence of recombinant Cdc25B. The fluorescence spectra of 0.2 µM Cdc25B in the absence or in the presence of the indicated concentrations of **7j** (A), **7i** (B) or **6e** (C) were recorded, normalised and corrected as indicated in Materials and Methods. An identical 1% (v/v) final concentration of DMSO is present in all samples. The data of fluorescence emission at 357 nm obtained in the absence (F_0) or in the presence of each inhibitor concentration (F_I) for **7j** (D), **7i** (E) or **6e** (F) were treated according to the Stern–Volmer equation.

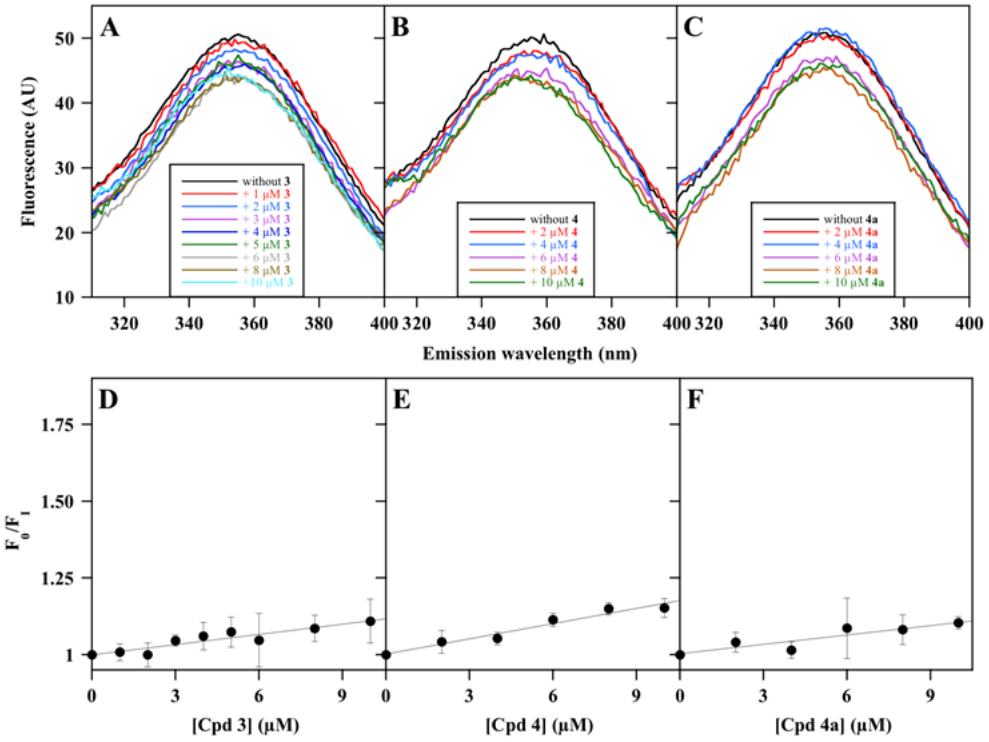

Figure 9. Effect of some uncompetitive inhibitors on the intrinsic fluorescence of recombinant Cdc25B. The fluorescence spectra of 0.2 µM Cdc25B in the absence or in the presence of the indicated concentrations of **3** (A), **4** (B) or **4a** (C) were recorded, normalised and corrected as indicated in Materials and Methods. An identical 1% (v/v) final concentration of DMSO is present in all samples. The data of fluorescence emission at 357 nm obtained in the absence (F_0) or in the presence of each inhibitor concentration (F_I) for **3** (D), **4** (E) or **4a** (F) were treated according to the Stern–Volmer equation.

4.6 Effect of some NSC28620 derivatives on the intrinsic fluorescence of Cdc25B-C473S in the absence or in the presence of OMFP

The data of the intrinsic fluorescence experiments obtained with inhibitors **3**, **4** and **4a** suggest that these **NSC28620** derivatives were unable to form a stable Cdc25B•inhibitor complex in the absence of substrate. To verify the possible formation of this complex in the presence of OMFP the mutant Cdc25B-C473S turned to be useful, because this enzyme binds OMFP, but does not catalyse its hydrolysis. Hence, the effects produced by the uncompetitive inhibitors **3**, **4** and **4a**, as well as by the noncompetitive inhibitor **7j**, on the intrinsic fluorescence of Cdc25B-C473S in the absence or in the presence of 5 μM OMFP were investigated. In the absence of OMFP, the uncompetitive inhibitors cause a very low dose-dependent quenching of the Cdc25B-C473S emission, similar to that exhibited by the wild-type Cdc25B; on the other hand, in the presence of a saturating OMFP concentration, besides a roughly 50% reduction of fluorescence yield due to the quenching by the substrate, the inhibitors cause a consistent dose-dependent quenching, as better evaluated through the Stern-Volmer plots (Figure 10A→C). In the absence of OMFP, low values of K_{SV} were obtained (0.019 μM^{-1}, 0.008 $\mu M^{-1}$and 0.011 $\mu M^{-1}$for **3**, **4** and **4a**, respectively), similar to those measured with the wild-type Cdc25B. This finding confirms that also the Cdc25B-C473S mutant enzyme has a very weak interaction with these uncompetitive inhibitors. On the other hand, slopes of the straight lines substantially rise in the presence of OMFP and the measured values of K_{SV} increase to 0.042 μM^{-1}, 0.023 μM^{-1} and 0.031 μM^{-1} for **3**, **4** and **4a**, respectively. The corresponding values of K'_D (24 μM, 43 μM and 32 μM for **3**, **4** and **4a**, respectively) indicate that OMFP strengthens the weak interaction of the enzyme with these uncompetitive inhibitors. Besides this relevant role of the substrate, the K'_D values of the uncompetitive inhibitors

remain greater than those obtained for noncompetitive inhibitors, a finding probably reflecting the lower inhibition power exhibited by uncompetitive respect to noncompetitive inhibitors.

The effects on the intrinsic fluorescence of Ccd25B-C473S in the absence or in the presence of OMFP were evaluated even for the noncompetitive inhibitor **7j**. As expected, the dose-dependent quenching of the intrinsic fluorescence was evident without or with OMFP. Indeed, the straight lines of the corresponding Stern-Volmer plots obtained were almost overlapping either in the absence or in the presence of OMFP (Figure 10D). Therefore, these data confirm that the direct interaction between enzyme and inhibitor **7j** occurs in the absence of the substrate and it is not affected when the substrate binding pocket is occupied.

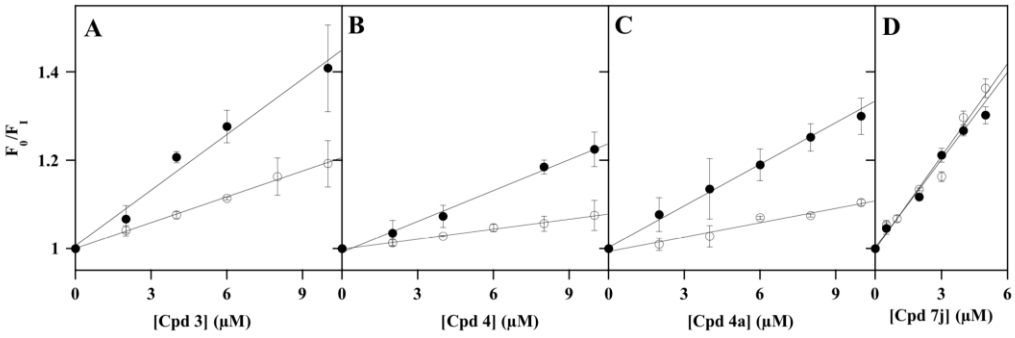

Figure 10. Effect of some inhibitors on the intrinsic fluorescence of recombinant Cdc25B-C473S in the absence or in the presence of OMFP. The data of fluorescence emission at 357 nm used for drawing the Stern–Volmer plots were obtained from the fluorescence spectra, recorded with the same protocol described in the legend to Figures 8 and 9. The F_0/F_I ratios were calculated in the presence of the indicated concentrations of **3** (A), **4** (B), **4a** (C) or **7j** (D) either in the absence (open circles) or in the presence of 5 μM OMFP (filled circles).

4.7 Evaluation of the effect of NSC28620 derivatives on the cell growth rate of melanoma cells

Previously it was demonstrated that the lead compound **NSC28620** affected the cell cycle, increased the protein levels of the inactive p-Cdk1, as well as reduced the cell viability of some cancer cell lines (Lavecchia et al. 2012). Hence, the action exerted by the **NSC28620** derivatives in human melanoma cell lines, a highly resistant and aggressive cancer type, was evaluated. In particular, the effects of these compounds on the cell growth of A2058 melanoma cell line were detected after different times of treatment with 50 μM of inhibitors, by means the MTT assay. Only one compound, **4a**, caused an evident cytotoxic activity after 24 h of treatment, but when the analysis was prolonged at 48 h of treatment also another compound, that is **4**, became cytotoxic (data not shown).

In order to check the minimum concentration of **4** and **4a** that induces a reduction of the cell growth rate, the time-dependent effect of these compounds on A2058 melanoma cells was tested at lower concentrations, *i.e.* 2.5 and 5 μM (Figure 11, panels A and B). The data show that, at low concentrations, only the **4a** exerted a progressive reduction of cell viability. In particular, after 48 h of incubation with 5 μM, **4a** reduced significantly the cell growth, and after 72-h treatment, even at concentration of 2.5 μM the cell growth was significantly affected (Figure 11B). In addition, we have then checked the possible cytotoxic effect exerted by compound **4a** in normal cells, such as the nonmalignant human fibroblast cell line BJ-5ta (Figure 11C). The results of MTT assay, performed at different concentrations and prolonged up to 72 h, indicates that compound **4a** was not cytotoxic for this nontumor cell line, even at 10 μM, a two fold concentration than the one used on cancer cells. Fibroblasts were chosen because of their consistent and ubiquitous presence in any body tissue; the non-cytotoxicity of **4a** in BJ-5ta leads to hypothesize that this compound could not provoke unspecific toxic side-effects in a normal cellular context.

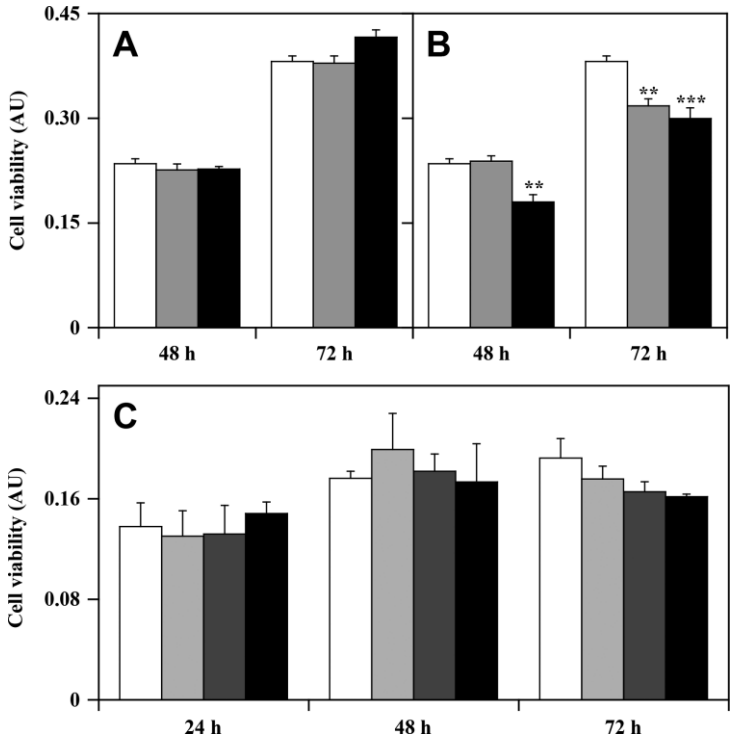

Figure 11. Cell toxicity of the compound 4 and 4a. Panels (A,B) A2058 cells were incubated for 48 or 72 h with 0.5% (v/v) DMSO (open bars), 2.5 μM (gray bars) or 5.0 μM (black bars) of compound **4** (panel A) or **4a** (panel B). Panel (C) BJ-5ta cells were incubated for 24, 48, or 72 h with 0.5% (v/v) DMSO (open bars), 2.5 μM (light gray bars), 5.0 μM (darkgray bars), or 10 μM (black bars) of compound **4a**. Data of cell viability were obtained from at least three independent experiments and expressed in arbitrary units, as the mean ± SE. **, $p < 0.01$; ***, $p < 0.001$ compared to control cells.

Hence, compound **4a** was chosen for further biological studies to better investigate its cytotoxicity in melanoma cell lines. The capability to form cell clones, an intrinsic characteristic of tumors cells was evaluated in the presence of **4a**. To this aim, the colony formation assay was performed to evaluate the long-term cell growth inhibitory effect of **4a** in melanoma cells. A2058 and A375 melanoma cell lines were treated with various concentrations of **4a** (0-10 μM) and colony formation was monitored. As shown in Figure 12, the compound **4a** affected colony formation in a dose-dependent manner. Indeed, the number of cell clones progressively decreased by increasing the

concentration of **4a** (0.625, 1.25, and 2.5 μM) and was almost absent in the presence of 5 or 10 μM inhibitor in both cell lines.

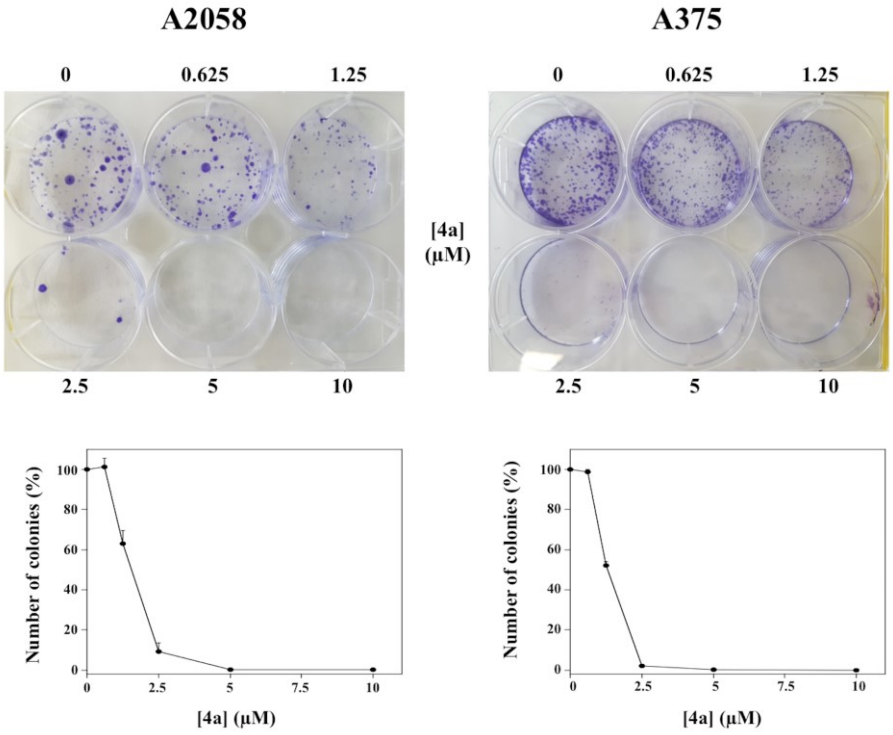

Figure 12. Effect of 4a on the colony formation of melanoma cells. A2058 and A375 cells were treated with vehicle alone or 0.625, 1.25, 2.5, 5.0, or 10 μM **4a**. After 10 days treatment, plates were photographed and images of representative experiments are shown. The bottom plots report the number of colonies counted as indicated in Materials and Methods; values are expressed in percentages and reported as the mean ± SE from at least three different experiments.

4.8 Evaluation of the effect of 4a on cell cycle progression and p-Cdk1 level

A deeper investigation was conducted to study the mechanisms involved in the toxic action of **4a** in melanoma cells. Cdc25 enzymes play a pivotal role in the regulation of the cell cycle, as well as in the control of DNA damage (Boutros et al. 2006). For this reason, the inhibitory potential of **4a** toward the Cdc25B phosphatase activity leads to hypothesize that this compound could induce a cell cycle arrest in cultured cells. Hence, we evaluated the effect of **4a** on cell cycle progression, by treating both A2058 and A375 melanoma cells with 10 μM **4a** for 8 and 16 h and then the cell cycle phase distribution was detected through cytofluorimetry after propidium iodide (PI) staining (Figures 13 and 14). In particular, after 8 h of treatment with **4a**, in both A2058 (Figure 13A,C) and A375 (Figure 14A,C) cells a significant reduction of the percentage of cells in G0/G1 phase and an increase of cell percentage in G2/M phase was observed. Instead, when the incubation was prolonged up to 16 h, a somehow different response emerged from the two cell lines. In A2058 cells, a further increase of cell percentage arrested in G2/M was evident, as well as an ulterior decrease of cells in the G0/G1 phase, together with a small non-significant increase of the sub G1 phase (Figure 13B,D). On the other hand, in A375 cells, the cell number arrested in the G2/M phase was similar between treated and untreated cells, the reduction of the cells in the G0/G1 phase was still evident but less pronounced compared to 8 h treatment, but interestingly, the increase of the sub G1 phase became greatly significant, compared to untreated cells (Figure 14B,D).

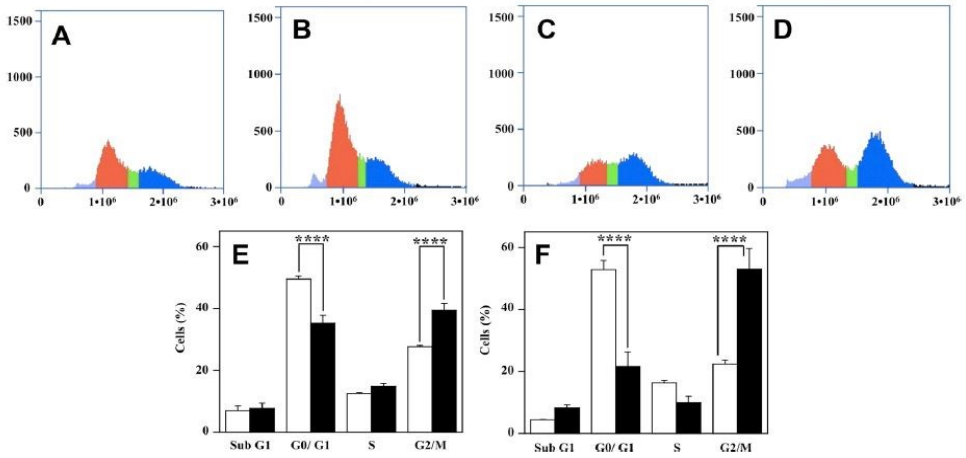

Figure 13. Effect of 4a on the distribution of cell cycle phases of A2058 cells. The distribution of cells in the different phases was evaluated after 8 h (panels A,C) or 16 h (panels B,D) from treatment with 0.5% DMSO (panels A,B) or 10 μM **4a** (panels C,D) as described in Materials and Methods. Cell cycle phases colours: sub G1, light blue; G0/G1, red; S, green; G2/M, dark blue. Histograms show the cell percentage distribution among the various phases after 8 h (panel E) or 16 h (panel F). Data obtained from triplicate experiments in the presence of DMSO (open bars) or **4a** (black bars) are reported as the mean ± SE. ****, $p < 0.0001$ compared to control cells.

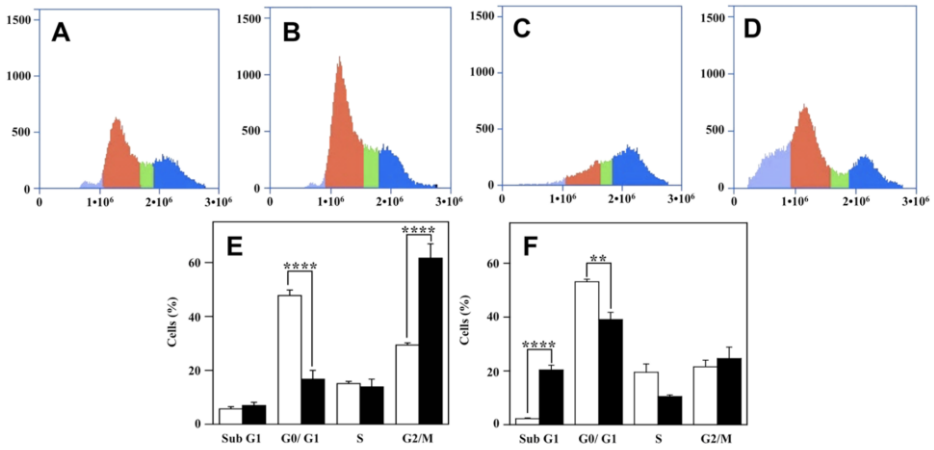

Figure 14. Effect of 4a on the distribution of cell cycle phases of A375 cells. The same protocol described in the legend to Figure 13 was followed to analyze the cell phases distribution of A375 cells. **, $p < 0.01$; ****, $p < 0.0001$ compared to control cells.

The arrest in G2/M of both melanoma cell lines induced by **4a** could indicate that this compound exerts its inhibitory capacity toward Cdc25 phosphatases also in cellular systems. Cell cycle progression is regulated by Cdc25 phosphatases through the dephosphorylation and then activation of Cdks (Rudolph 2007; Aressy and Ducommun 2008). In particular, because Cdk1 is a key regulator of G2/M transition, the dephosphorylation of its inactive form, p-Cdk1, represents a critical event for the entry into mitosis (Morgan 1995; Hoffmann et al. 1993; Yamaura et al. 2009). Hence, we tested if the treatment of melanoma cells with **4a** could affect the protein levels of p-Cdk1. Indeed, in both A2058 and A375 melanoma cells, after 8 h of treatment with **4a** the levels of the phosphorylated and inactive form of Cdk1 are significantly higher respect to that of untreated cells (Figure 15).

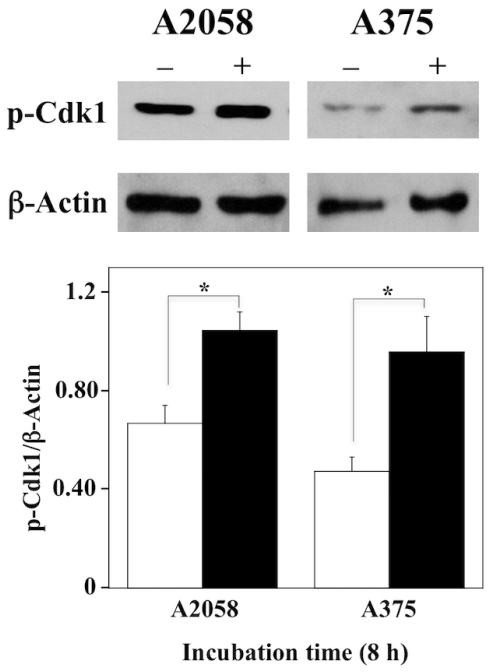

Figure 15. Effect of 4a on p-Cdk1 protein levels. A2058 and A375 cells were incubated in the absence or in the presence of 10 μM **4a** for 8 h and total protein extracts were used to detect p-Cdk1 levels through western blot. β-Actin was used as an internal loading control. *, $p < 0.05$ compared to control cells.

4.9 Evaluation of pro-apoptotic effect of compound 4a in melanoma cells

The arrest of melanoma cells in G2/M phase provoked by **4a** suggests that this compound could exert its cytotoxic action by inducing an apoptotic program. It is known that the arrest of the cell cycle in G2/M phase can occur in case of DNA damage to permit the mutations repair (Rudolph 2007). If the G2/M phase block is prolonged and the DNA damages are not fixed, the cells can undertake an apoptotic program to prevent the transmission of mutations to the daughter cells (Campisi et al. 2007). Thus, we evaluated the pro-apoptotic effect of **4a** in melanoma cells. To this aim, A2058 and A375 cells were treated with 5 or 10 μM **4a** for different times and the apoptosis was monitored cytofluorimetrically after PI incorporation. As shown in Figure 16, a dose- and time-dependent increase of cell percentage with a hypodiploid DNA content was evident in both cell lines. In particular, the increment of apoptosis was already significant after 48-h treatment with 5 or 10 μM **4a** and became more pronounced after 72-h treatment, in both A2058 (Figure 16A) and A375 (Figure 16B) melanoma cells. The pro-apoptotic effect of **4a** was evaluated also in the nontumorigenic fibroblast cell line BJ5ta. The data obtained show that **4a** did not exert any apoptotic effect in these nonmalignant cells up to 72 h of treatment (Figure 16C).

A further investigation on the pro-apoptotic effect of compound **4a** in melanoma cells was performed by measuring the enzymatic activity of caspase-3 and caspase-9, representing the final effector of apoptosis and one of the main mediators of the intrinsic apoptotic program, respectively (Degterev et al. 2003). Cell treatment with 10 μM **4a** induced a statistically significant increase of enzymatic activity of caspase-3 (Figure 17A,B) and caspase-9 (Figure 17C,D) in both melanoma cell lines. To verify if the apoptosis induced by **4a** in melanoma cells was caspase-mediated, the cytofluorimetric analysis of the apoptosis was evaluated in cells incubated with Z-VAD-FMK, an

irreversible pan-caspase inhibitor. Hence, melanoma cells were treated for 48 h with 10 μM **4a** in the presence or in the absence of Z-VAD-FMK. The data shown in Figure 17E,F indicate that in the presence of the caspase inhibitor a partial but significant reduction of the apoptosis level occurs in both melanoma cell lines.

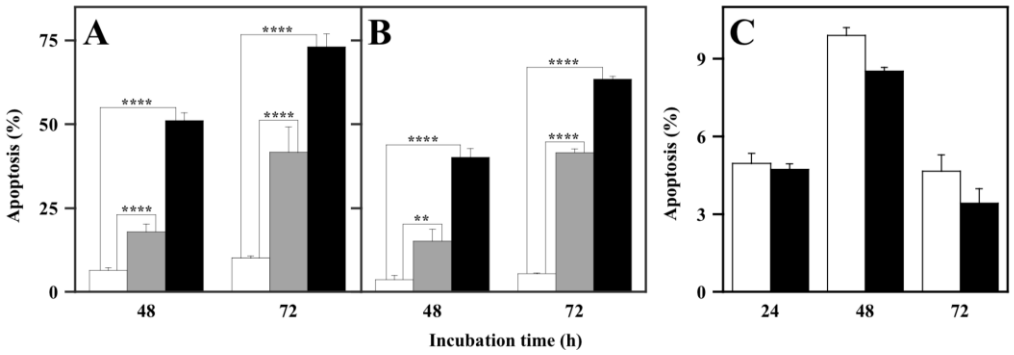

Figure 16. Apoptotic effect of 4a in A2058, A375 and BJ-5ta cell lines. A2058 (A), A375 (B) and BJ-5ta (C) cells were treated with 0.5% (v/v) DMSO (white bars), 5 μM **4a** (grey bars) or 10 μM **4a** (black bars), and apoptosis was evaluated after the indicated incubation time through the determination of the number of cells with a subdiploid DNA content. Data from triplicate experiments were expressed as a percentage and reported as the mean ± SE. **, $p<0.01$; ****, $p<0.0001$ compared to untreated cells.

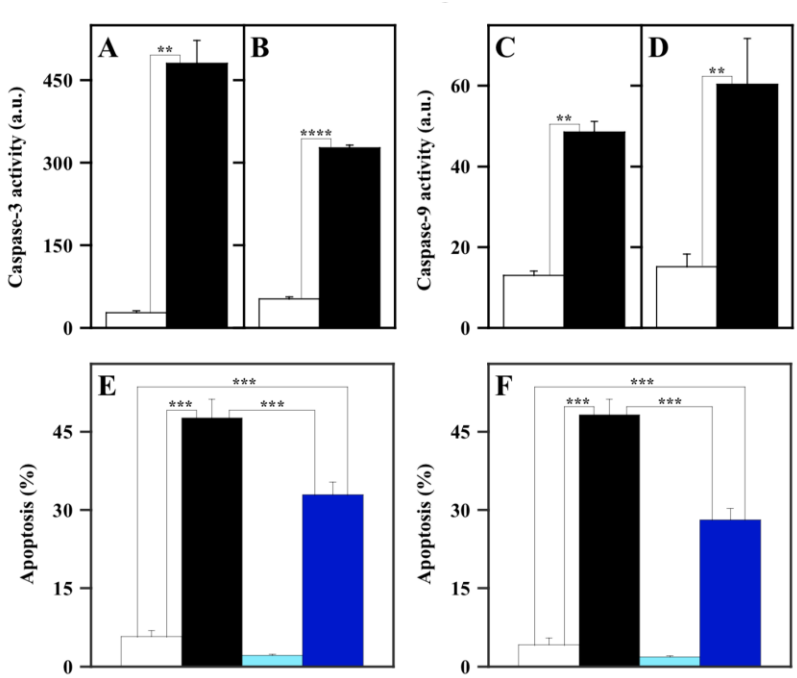

Figure 17. Involvement of caspase-3 and -9 in the apoptotic program induced by 4a in melanoma cells. (A, B, C, D) Effect of **4a** on the caspase-3 and caspase-9 activity in melanoma cells. A2058 (A, C) and A375 (B, D) cells were incubated for 24 h with 0.5% (v/v) DMSO (white bars) or 10 µM **4a** (black bars). The enzymatic activity of caspase-3 (A, B) and caspase-9 (C, D) was reported as arbitrary units (a.u.). Data from triplicate experiments were reported as the mean ± SE. **, $p<0.01$; ****, $p<0.0001$ compared to untreated cells. (E, F) Effect of Z-VAD-FMK, a pan-caspase inhibitor, on the apoptosis induced by **4a** in melanoma cells. A2058 (E) and A375 (F) cells were incubated for 48 h with 0.5% (v/v) DMSO (white bars), 10 µM **4a** (black bars), 100 µM Z-VAD-FMK (cyan bars) or 10 µM **4a** plus 100 µM Z-VAD-FMK (blue bars). The apoptosis was evaluated through the determination of the number of cells with a subdiploid DNA content. Data from triplicate experiments were expressed as a percentage and reported as the mean ± SE. ***, $p<0.001$ compared to respective control cells.

The increment of caspase-9 activity induced by **4a** in melanoma cells suggests that the apoptosis could be mitochondria-mediated. Hence, to verify if **4a** induces a cytosolic translocation of the cytochrome *c*, one of the main events that leads to the intrinsic mitochondria-mediated apoptosis (Wolter et al. 1997), immunofluorescence and western blotting experiments were performed. A2058 and A375 cells, untreated or treated with 10 µM **4a**, were subjected to immunofluorescence labelling with an anti-cytochrome *c* antibody (Figure 18).

In untreated cells, cytochrome *c* (green signal) is essentially localised in the mitochondria (red signal), as confirmed by the yellow merged signal. On the other hand, treatment with **4a** induces a cytosolic translocation of cytochrome *c*, as clearly indicated by the appearance of green fluorescence in the cytosol.

Western blotting experiments, using fractioned protein extracts (cytosol and mitochondria) of melanoma cells incubated with **4a**, confirmed these results. Indeed, this compound induces a significant cytosolic translocation of cytochrome *c* in both A2058 (Figure 19A) and A375 (Figure 19B) cells.

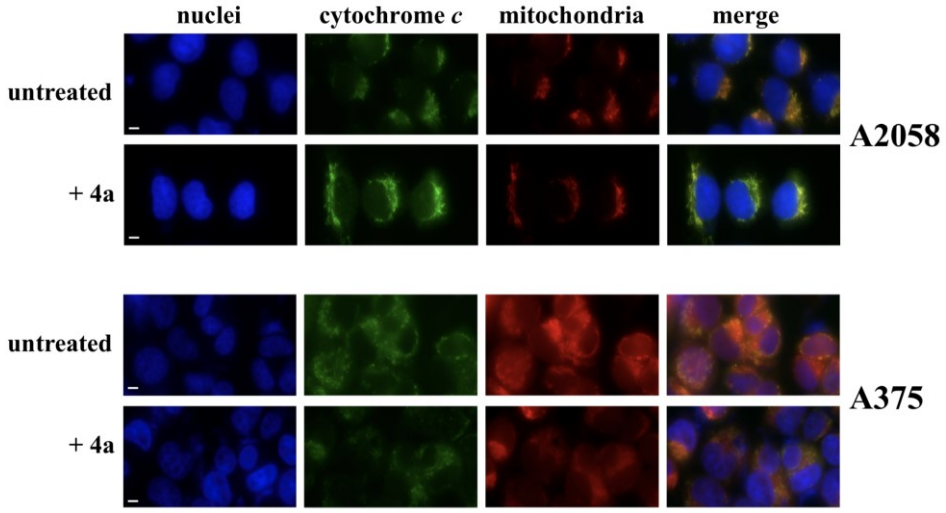

Figure 18. Immunofluorescence analysis of cytochrome *c* subcellular localisation in melanoma cells. A2058 and A375 cells were untreated (0.5% v/v, DMSO) or treated with 10 μM **4a** for 24 h. The cell nuclei were labelled with DAPI (blue channel); the cytochrome *c* immunofluorescent staining (green channel) was performed using a polyclonal anti-Cyt *c* antibody, followed by FITC-conjugated antibody; mitochondria were stained with MitoTracker Red (red channel). The degree of spatial overlap in cytochrome *c* immunostaining and MitoTracker Red staining is shown by yellow fluorescence, corresponding to merge of red and green channel. Scale bar, 10 μm; magnification x 40.

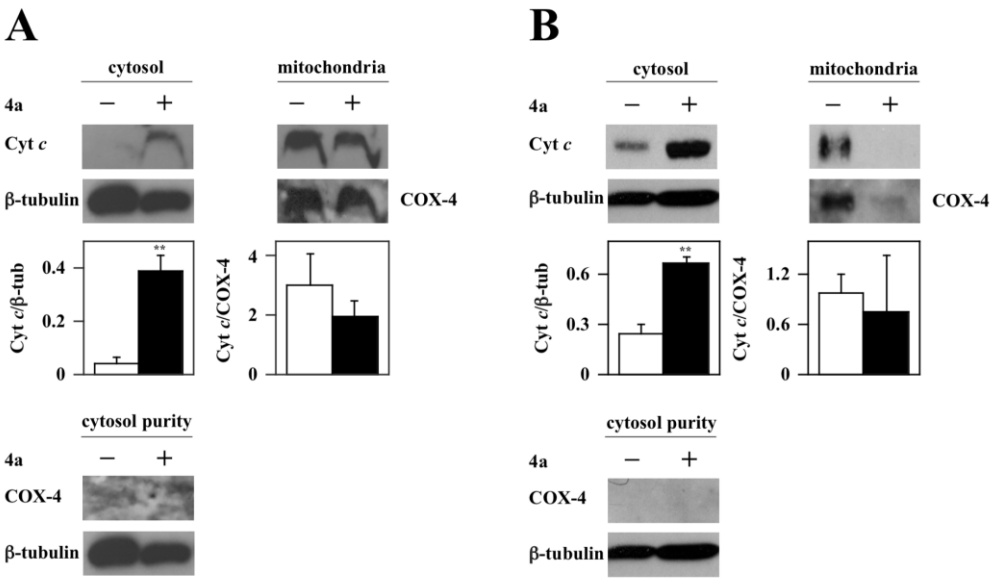

Figure 19. Effect of 4a on cytochrome *c* subcellular localisation in melanoma cells. A2058 (A) and A375 (B) cells were incubated for 24 h with 0.5% (v/v) DMSO (white bars) or 10 μM **4a** (black bars), and then the cytosolic and mitochondrial protein extracts were prepared for Western blotting analysis, using β-tubulin or COX-4 as loading controls of the cytosolic or mitochondrial fraction, respectively. Purity of the cytosolic fraction was monitored by using β-tubulin or COX-4 as specific cytosolic or mitochondrial marker, respectively. The densitometric evaluation of three independent experiments was reported as the mean ± SE. **, $p<0.01$ compared to untreated cells.

4.10 Evaluation of the effect of 4a on typical markers of cell cycle progression, apoptosis and proliferation

The effects of **4a** on the proliferation rate, cell cycle progression and apoptosis observed in melanoma cells prompted us to investigate on the influence of compound **4a** on the levels of typical markers of these processes. It is known that Cdc25s, beside to regulate the cell cycle, can negatively modulate some apoptotic pathways (Morgan 1995, Yamaura et al. 2009, Zacksenhaus et al. 2018). Hence, the **4a** inhibitory capacity towards Cdc25 activity can be linked to the effects observed in melanoma cells. To this aim, we also evaluated the protein levels of the three forms of Cdc25 (Cdc25A, -B and -C) during treatment of melanoma cells with **4a**. The results of western blotting experiments (Figure 20) show a reduction of protein levels of the three forms of Cdc25 in both A2058 and A375 cells, essentially after 24- and 48 h of treatment with **4a**.

The tumor suppressor p53, named the "genome guardian", exerts a pivotal role in the control of genome integrity. In particular, this protein regulates key mechanisms involved in the eradication of damaged cells, exerting a fundamental role during neoplastic transformation (Agrawal et al. 2017). Hence, we have evaluated the protein levels of p53 after treatment of melanoma cells with **4a**. As shown in Figure 21, a clear and significant increase of p53 is evident in A2058 and A375 melanoma cells after 16- and 24-h treatment with **4a.**

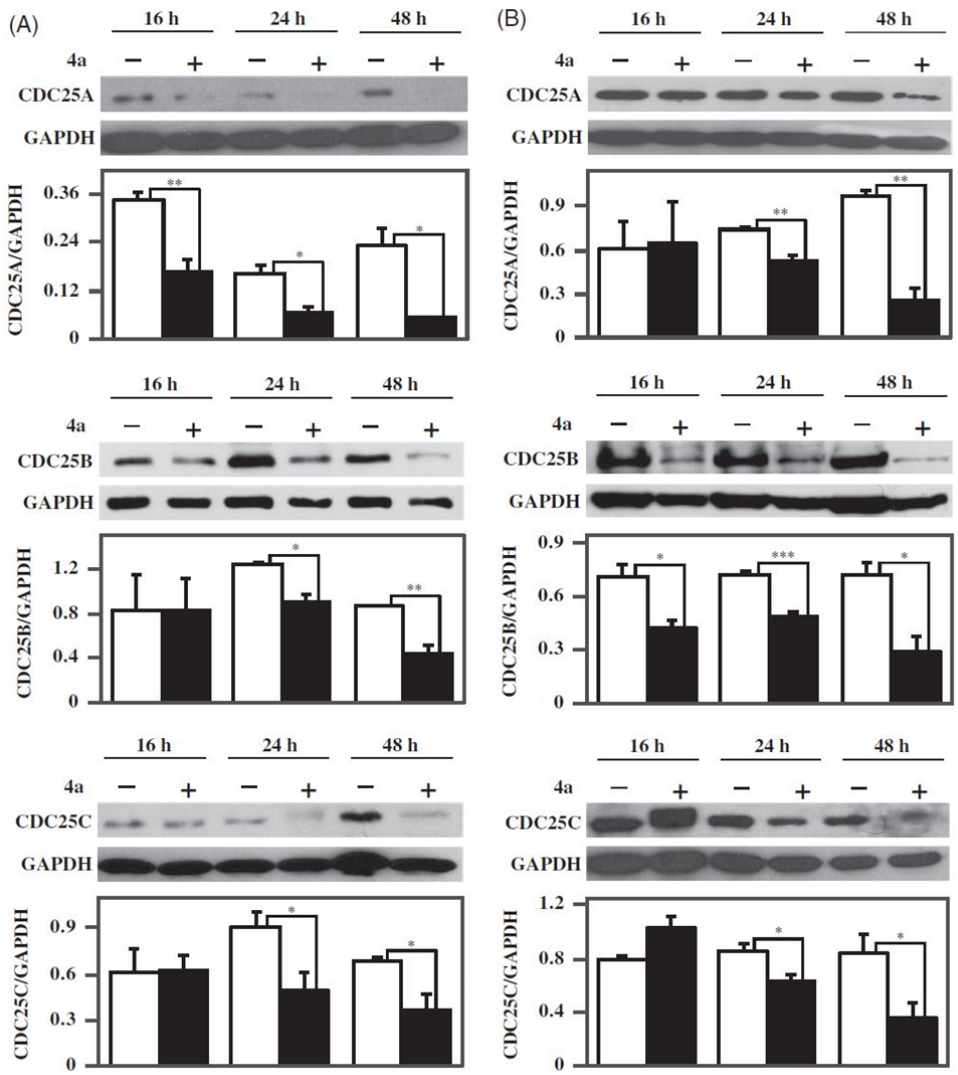

Figure 20. Effect of 4a on Cdc25A, -B and -C protein levels in melanoma cells. A2058 (A) and A375 (B) cells were incubated with 0.5% (v/v) DMSO (white bars) or 10 μM **4a** (black bars) for the indicated incubation time. Western blotting analysis was performed on total cellular extracts, using GAPDH as loading control. The densitometric evaluation of three independent experiments was reported as the mean ± SE. *, $p<0.05$; **, $p<0.01$; ***, $p<0.001$ compared to untreated cells.

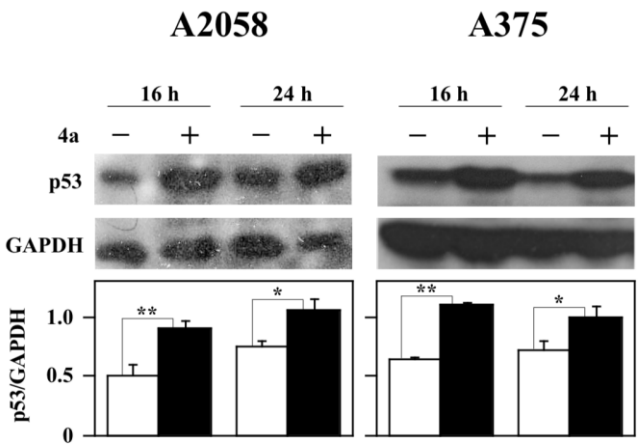

Figure 21. Effect of 4a on p53 protein levels in melanoma cells. A2058 and A375 cells were incubated with 0.5% (v/v) DMSO (white bars) or 10 μM **4a** (black bars) for the indicated incubation time. Western blotting analysis was performed on total cellular extracts, using GAPDH as loading control. The densitometric evaluation of three independent experiments was reported as the mean ± SE. *, $p<0.05$; **, $p<0.01$ compared to untreated cells.

It is known that a high percentage of melanomas harbour mutations in the BRAF gene (Ihle et al. 2014; Sullivan and Flaherty 2013). Hence, one of the main anti-melanoma strategies is the target therapy, by using B-Raf inhibitors. However, in many cases this treatment is not very successful because a great part of patients develop drug resistance (Ruocco et al. 2019). Targeted therapy resistance can be also due to the activation of other cell surviving pathways, bypassing the anti-proliferative effects of B-Raf inhibitors. Frequently in primary melanomas the phosphatidylinositol 3-kinase/protein kinase B (PI3K/AKT) pathway is activated (Ruocco et al. 2019). Hence, we evaluated the protein levels of pAkt in melanoma cells treated with the compound **4a**. A significant and early decrease of pAkt protein levels was observed in both melanoma cell lines after 30 minutes of treatment with **4a** (Figure 22). This finding suggests that the combined use of compound **4a** with conventional B-

Raf inhibitors can contribute to reduce the occurrence of therapy resistance in melanoma.

The molecular investigations on the action of **4a** in melanoma cells suggest that the cytotoxic effect of this compound could be related to the inhibition of Cdc25 activity/protein levels as well as the modulation of key cellular surviving pathways.

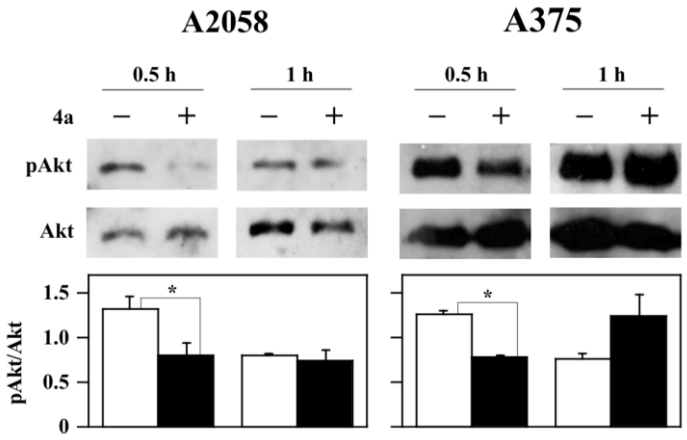

Figure 22. Effect of 4a on pAkt protein levels in melanoma cells. A2058 and A375 cells were incubated with 0.5% (v/v) DMSO (white bars) or 10 μM **4a** (black bars) for the indicated incubation time. Western blotting analysis was performed on total cellular extracts, using Akt as loading control. The densitometric evaluation of three independent experiments was reported as the mean ± SE. *, $p<0.05$ compared to untreated cells.

5. DISCUSSION

The aim of this thesis has been a biochemical and biological investigation on novel derivatives designed from the lead compound **NSC28620** (Lavecchia et al. 2012), in order to obtain more potent inhibitors of Cdc25 enzymes. The Cdc25 inhibitors belong to various chemical classes including phosphate bioisosteres, electrophilic entities, and most of them have a quinonoid structure (Tao et al. 2020). In particular, most quinonoid molecules act as potent and irreversible inhibitors of Cdc25s, but their consideration as anticancer agents is discouraged by possible side-toxic effects (Evain-Bana at al. 2017). To date, only a limited number of studies described the identification of Cdc25 inhibitors based on non-quinonoid structures (Lavecchia et al. 2012; Rosenkera et al. 2015; Zwergel et al. 2017). **NSC28620** derivatives, characterized by a non-quinonoid structure, are particularly attractive because non-quinonoid molecules are intrinsically endowed with lower side-toxic effects.

The structural modifications made on the **NSC28620** scaffold produced a total of 31 derivatives, characterized by differences in their inhibition power and mechanism. Interestingly, some derivatives (**7j**, **7i**, **6e**, **7f**, and **3**) showed a higher inhibitory activity compared to the lead **NSC28620**, with the most potent inhibitor **7j** being 7-fold more active (K_i, 0.8 μM) towards Cdc25B. However, it is likely that these **NSC28620** derivatives are also active on Cdc25A and -C, as suggested by the inhibition properties of **7j** and **3** on the recombinant forms of Cdc25A and -C. It is known that the lead **NSC28620** acts as a competitive inhibitor of the three Cdc25 forms (Lavecchia et al. 2012). However, based on the kinetic data of phosphatase inhibition, the 31 derivatives were putatively assigned to different categories of inhibition mechanism. In particular, the novel compounds could be ranked in three groups of inhibitors, i.e noncompetitive, uncompetitive or mixed. In order to confirm this hypothesis, intrinsic fluorescence experiments were performed thanks to the presence of a single tryptophan residue (W550) in the catalytic

domain of Cdc25B. In particular, the interaction between Cdc25B and inhibitor was investigated by evaluating the effects caused by an increasing concentration of some representative members of noncompetitive (**7j**, **7i** and **6e**) and uncompetitive (**3**, **4** and **4a**) inhibitors on the intrinsic fluorescence of the recombinant enzyme. We also took advantage of the usage of a mutant form of Cdc25B (C473S-Cdc25B), able to bind the substrate OMFP, but unable to hydrolyse it. Indeed, with this mutant it was possible to study the interaction between enzyme and inhibitor even in the presence of OMFP, without the complication of its hydrolysis. The fluorescence studies proved that the putative noncompetitive inhibitors **7j**, **7i** and **6e** are capable to quench the fluorescence yield of Cdc25B and therefore directly interact with the enzyme, being capable to form the enzyme•inhibitor binary complex in the absence of the substrate; however, the formation of this complex is not affected when OMFP is previously bound to the mutant enzyme, as shown for **7j**. These results confirm that **7j**, **7i** and **6e** are endowed with a noncompetitive inhibition mechanism. Indeed, this categorization means that these compounds cause the inhibition, being capable to bind the enzyme (in a site different from the substrate binding pocket) either in the absence or in the presence of OMFP. On the other hand, for the uncompetitive inhibitors **3**, **4** and **4a** the presence of the substrate OMFP is required to strengthen an otherwise weak direct interaction between enzyme and inhibitor. In other words, **3**, **4** and **4a** may form a ternary complex, enzyme•OMFP•inhibitor, because the binding of the substrate is needed to permit a stable enzyme inhibitor interaction. Therefore, these data confirm that these compounds approach the mechanism of inhibition ranked as uncompetitive, meaning that these compounds cause the inhibition, being capable to bind the enzyme only in the presence of OMFP. In the complex, the combination of kinetic studies of Cdc25B phosphatase inhibition by **NSC28620** derivatives and fluorimetric investigations on their binding interaction with the enzyme led to a detailed understanding of the inhibition mechanism of these small molecules based on a direct (noncompetitive) or

substrate-mediated (uncompetitive) interaction with the target enzyme. Furthermore, the finding that three members of the same group of inhibitors keep a fluorimetric behaviour specific for the type of inhibition might point to the statistical relevance of this investigation, thus allowing an enlargement of the assignment (noncompetitive or uncompetitive inhibition) to the other **NSC28620** derivatives.

It is note that melanoma represents one of the most deadly skin tumors, highly refractory to conventional therapies (Uzdensky, et al. 2013). Hence, many studies are devoted to the discovery of new drugs for the treatment of this cancer by targeting various signaling pathways and attacking elements that underlie the tumor's propensity for growth and chemoresistance (Irwin et al. 2012). As Cdc25 phosphatases, key regulators of cell cycle, are overexpressed in many tumors, including melanoma (Boutros et al. 2007), we evaluated the effect of these inhibitors on the cell growth rate of A2058 melanoma cells. This screening revealed that only the compound **4a** induces, at low concentrations (5-10 μM), a significant reduction of melanoma cell viability. Instead, **NSC28620** exerts its toxic effect at higher doses (200 μM) and in more responsive tumor cell lines (Lavecchia et al. 2012). Hence, the compound **4a** was chosen for further biological studies to better investigate on its cytotoxic mechanism in melanoma cell lines. The inhibitory potential of **4a** toward Cdc25 phosphatase activity suggests that this compound can provoke a cell cycle arrest in melanoma cells. Indeed, we have observed that compound **4a** causes an alteration of the cell cycle in both A2058 and A375 melanoma cell lines. However, the two cell lines showed a different response to **4a** treatment. After an initial (8 h) similar behaviour, represented by an increase of G2/M phase concomitant to a reduction of G0/G1 phase, at a later time (16 h) a significant sub G1 phase associated to a reduction of G2/M phase appeared only in A375 cells, whereas for A2058 the increase of G2/M phase continued. The arrest in G2/M could represent a cellular response to the toxic effect of **4a**, perhaps mediated by the Cdc25 inhibition; however, this effect can evolve in

cell death after a prolonged treatment, as suggested by the behavior of A375 cells. It is note that the entry in each phase of cell cycle is strictly supervised by cell-cycle checkpoint systems that are responsible for the arrest of cell cycle, as a response to DNA damage. A block in G2/ M phase prevents the entry into mitosis, thus allowing the onset of a number of processes devoted to repair the DNA damage. The activation of Cdc25 phosphatases, in particular Cdc25C, is crucial for the progression through G2/M checkpoint (DiPaola 2002). Hence, the inhibition of Cdc25s can contribute to the arrest of cell cycle in G2/M phase; however, if the arrest is prolonged and the DNA damage is not repaired, cells can activate an apoptotic programme in order to avoid the transfer of DNA mutated to daughter cells (Campisi and d'Adda di Fagagna 2007). Our data clearly indicate that the treatment of melanoma cells with **4a** activates an apoptotic program, mainly mitochondria mediated. Indeed, the compound **4a** induced an increase of cells with a hypodiploid content of DNA, an increment of caspase-9 and caspase-3 activity linked to a cytosolic translocation of cytochrome *c*. Hence, we can infer that the apoptosis induced by **4a** in melanoma cells represents a consecutive process to the long cell cycle blockage in the G2/M phase. Furthermore, the increase of protein level of the inactive form of Cdk1, p-Cdk1, suggests that the behaviour of melanoma cells could be due to the inhibition potency of **4a** toward Cdc25 activity also in a cellular system. It is important to note that Cdc25s exert an anti-apoptotic role, by suppressing some apoptotic pathways either directly or indirectly. Indeed, Cdc25 inhibits Apoptosis Signal-regulating Kinase (ASK1) as well as inhibits apoptosis through the activation of Cdk1, which in turn phosphorylates and inactivates caspase-9 (Morgan 1995; Yamaura 2009; Zacksenhaus et al. 2018). Hence, the reduction of protein levels of Cdc25A, -B and -C induced in melanoma cells during treatment with **4a** can contribute to activate an apoptotic program.

Melanoma represents one of the most aggressive skin tumors. Indeed, when diagnosed in a later phase it is very refractory to conventional therapies. It is

known that anti-melanoma target strategies are based on the usage of B-Raf inhibitors, which selectively inhibit the proliferation of melanoma cells harbouring the BRAF mutations (Ruocco et al. 2019). However, the success of this therapy is not definitive, because usually the patients relapse because of acquired drug resistance, possibly due to the activation of others survival pathways. The use of B-Raf inhibitors paradoxically activates the Akt signalling pathway, which promotes the tumour survival of B-Raf-mutant melanoma cells (Gopal et al. 2010; Perna et al. 2015). Furthermore, in tumor cells, the UV exposure can activate the PI3K/AKT-dependent mechanism that stabilises Cdc25A and induces its translocation into the cytoplasm, where it does not affect the cell cycle progression, but acts as anti-apoptotic factor (Holmes et al. 2019). On the other hand, it has been observed that Cdc25B mediates the activation of Akt, probably through the dephosphorylation of specific protein kinases (Chen et al. 2009). It is important to note that Akt phosphorylates and then activates MDM2, a typical inhibitor of p53 (Feng at al. 2004). Frequently, in melanoma the gene encoding p53 is not mutated, but its reduced function depends on high levels of the phosphorylated form of MDM2 (Lu et al. 2013). Hence, the early decrease of pAkt levels could be linked to a concomitant impairment of Cdc25 activity and furthermore, the reduced activity of Akt could provoke the increase of p53 level. In the complex, we can speculate that these molecular events can mediate the toxic effect exerted by **4a** in melanoma cells.

6. CONCLUSIONS

Melanoma, the most deadly of all skin tumors, results from complex changes in multiple signaling pathways that control the cell proliferation and the ability to evade the cell death processes. In this tumour, as in other cancers, loss of cell cycle regulation contributes to uncontrolled proliferation. Some compounds that arrest the cell cycle and promote apoptosis of melanoma cells are currently tested as promising anti-melanoma drugs (Uzdensky et al. 2013). In particular, the deregulation of Cdc25s in melanoma cells suggests that this crucial element of cell cycle could be considered as a possible oncotarget *in vivo*. Hence, molecules that displayed an inhibitory action on Cdc25 enzymatic activity could contribute to the development of new therapeutic strategies. In particular, among Cdc25 inhibitors, compounds with the **NSC28620** scaffold are particularly attracting for the design of molecules endowed with potential anticancer properties, because their non-quinonoid structure can reduce the unspecific side toxic effects usually observed with the most known quinonoid Cdc25 inhibitors. Our biochemical studies on the inhibition mechanism of **NSC28620** derivatives as well as the biological evaluation of the effects exerted by **4a**, a highly cytotoxic member of these molecules, improve the basic knowledge on Cdc25 inhibitors and represent the starting point for the discovery and production of more potent bioactive molecules. Indeed, the development of molecules with a high specificity against selected cancer cells, minimum undesired side toxic effects and reduced appearance of drug resistance represents one of the main objectives of drug discovery studies. In this regard, the compound **4a** is very interesting because it exerts a specific toxic effect in melanoma cells at low concentration, affecting alternative survival pathways responsible for the acquirement of drug resistance usually observed during the therapeutic treatment of melanoma with conventional agents.

In the complex, the discovery and production of more potent bioactive molecules, can contribute to the development of anticancer strategies based on the cotreatment of melanoma with different drugs targeting independent survival pathways or the combination of multitargeted therapy and immunotherapy.

7. LIST OF PUBLICATIONS:

1. Angelica Avagliano, Maria Rosaria Ruocco, **Federica Aliotta**, Immacolata Belviso, Antonello Accurso, Stefania Masone, Stefania Montagnani, Alessandro Arcucci. Mitochondrial Flexibility of Breast Cancers: A Growth Advantage and a Therapeutic Opportunity. Cells 2019; 8(5):401.

2. Carmen Cerchia, Rosarita Nasso, Matteo Mori, Stefania Villa, Arianna Gelain, Alessandra Capasso, **Federica Aliotta**, Martina Simonetti, Rosario Rullo, Mariorosario Masullo, Emmanuele De Vendittis, Maria Rosaria Ruocco, Antonio Lavecchia. Discovery of Novel Naphthylphenylketone and Naphthylphenylamine Derivatives as Cell Division Cycle 25B (CDC25B) Phosphatase Inhibitors: Design, Synthesis, Inhibition Mechanism, and in Vitro Efficacy against Melanoma Cell Lines. J Med Chem 2019; 62(15):7089-7110.

3. Angelica Avagliano, Maria Rosaria Ruocco, Rosarita Nasso, **Federica Aliotta**, Gennaro Sanità, Antonino Iaccarino, Claudio Bellevicine, Gaetano Calì, Giuseppe Fiume, Stefania Masone, Mariorosario Masullo, Stefania Montagnani, Alessandro Arcucci. Development of a Stromal Microenvironment Experimental Model Containing Proto-Myofibroblast Like Cells and Analysis of Its Crosstalk with Melanoma Cells: A New Tool to Potentiate and Stabilize Tumor Suppressor Phenotype of Dermal Myofibroblasts. Cells 2019; 8:1435.

4. **Federica Aliotta**, Rosarita Nasso, Rosario Rullo, Alessandro Arcucci, Angelica Avagliano, Martina Simonetti, Gennaro Sanità, Mariorosario Masullo, Antonio Lavecchia, Maria Rosaria Ruocco, Emmanuele De Vendittis. Inhibition mechanism of naphthylphenylamine derivatives acting on the CDC25B dual phosphatase and analysis of the molecular processes involved in the high cytotoxicity exerted by one selected derivative in melanoma cells. J Enzyme Inhib Med Chem 2020; 35(1):1866-1878.

5. Nicola Landi, Maria Rosaria Ruocco, Sara Ragucci, **Federica Aliotta**, Rosarita Nasso, Paolo V. Pedone, Antimo Di Maro. Quinoa as source of type 1 ribosome inactivating proteins: A novel knowledge for a revision of its consumption. Food Chem 2021; 342:128337.

6. Veronica Romano, Immacolata Belviso, Alessandro Venuta, Maria Rosaria Ruocco, Stefania Masone, **Federica Aliotta**, Giuseppe Fiume, Stefania Montagnani , Angelica Avagliano, Alessandro Arcucci. Influence of tumor microenvironment and fibroblast population plasticity on melanoma

growth, therapy resistance and immunoescape. Int J Mol Sci 2021; 22:5283.

8. REFERENCES

1. Agrawal SN, Dhruv K, Meshram S. p53: the guardian of genome, apoptosis, and its role in carcinogenesis. Eur J Biomed Pharm Sci 2017; 4(2):161-166.

2. Albano F, Arcucci A, Granato G, Romano S, Montagnani S, De Vendittis E, Ruocco MR. Markers of mitochondrial dysfunction during the diclofenac-induced apoptosis in melanoma cell lines. Biochimie 2013; 95(4):934-945.

3. Albert H, Santos S, Battaglia E, Brito M, Monteiro C, Bagrel D. Differential expression of CDC25 phosphatases splice variants in human breast cancer cells. Clin Chem Lab Med. 2011; 49(10):1707–1714.

4. Al-Matouq J, Holmes T, Hammiller B, Tran N, Holmes M, Freeman SC, Hansen AL. Accumulation of cytoplasmic CDC25A in cutaneous squamous cell carcinoma leads to a dependency on CDC25A for cancer cell survival and tumor growth. Cancer Lett. 2017; 410: 41-49.

5. Arcucci A, Ruocco MR, Amatruda N, Riccio A, Tarantino G, Albano F, Mele V, Montagnani S. Analysis of extracellular superoxide dismutase in fibroblasts from patients with systemic sclerosis. J Biol Regul Homeost Agents 2011; 25(4):647-654.

6. Arcucci A, Ruocco MR, Albano F, Granato G, Romano V, Corso G, Bancone C, De Vendittis E, Della Corte A, Montagnani S. Analysis of extracellular superoxide dismutase and Akt in ascending aortic aneurysm with tricuspid or bicuspid aortic valve. Eur J Histochem 2014; 58(3):2383.

7. Aressy B and Ducommun B. Cell Cycle Control by the Cdc25 Phosphatases. Anti-Cancer Agents Med. Chem. 2008; 8(8):818-824.

8. Arozarena I and Wellbrock C. Targeting invasive properties of melanoma cells. FEBS J 2017; 284(14):2148-2162.

9. Bhattacharjee H, Sheng J, Ajees AA, Mukhopadhyay R, Rosen BP. Adventitious Arsenate Reductase Activity of the Catalytic Domain of the Human Cdc25b and Cdc25c Phosphatases. Biochemistry 2010; 49(4):802-809.

10. Blomberg I And Hoffmann I. Ectopic expression of Cdc25A accelerates the G(1)/S transition and leads to premature activation of cyclin E- and cyclin A-dependent kinases. Mol Cell Biol 1999; 19(9):6183-6194.

11. Boudolf V, Inzé D, De Veylder L. What if higher plants lack a CDC25 phosphatase? Trends Plant Sci 2006; 11(10):474-479.

12. Boutros R, Dozier C, Ducommun B. The When and Wheres of Cdc25 Phosphatases. Curr Opin Cell Biol 2006;18(2):185-191.

13. Boutros R, Lobjois V, Ducommun B. CDC25 phosphatases in cancer cells: Key players? Good targets? Nat Rev Cancer 2007; 7(7):495-507.

14. Bradford MM. A rapid and sensitive method for the quantitation of microgram quantities of protein utilizing the principle of protein-dye binding. Anal Biochem 1976; 72:248-254.

15. Brenner AK, Reikvam H, Lavecchia A and Bruserud Ø. Therapeutic targeting the cell division cycle 25 (CDC25) phosphatases in human acute myeloid leukemia--the possibility to target several kinases through inhibition of the various CDC25 isoforms. Molecules 2014; 19(11):18414-18447.

16. Brezak M-C, Quaranta M, Contour-Galcera M-O, Lavergne O, Mondesert O, Auvray P, Kasprzyk PG, Prevost GP and Ducommun B. Inhibition of human tumor cell growth in vivo by an orally bioavailable inhibitor of CDC25 phosphatases. Mol Cancer Ther 2005; 4(9):1378-1387.

17. Brezak M-C, Valette A, Quaranta M, Contour-Galcera M-O, Jullien D, Lavergne O, Frongia C, Bigg D, Kasprzyk PG, Prevost GP, Ducommun B. IRC-083864, a novel bis quinone inhibitor of CDC25 phosphatases active against human cancer cells. Int J Cancer 2009; 124(6):1449-1456.

18. Brisson M, Nguyen T, Wipf P, Joo B, Day BW, Skoko JS, Schreiber EM, Foster C, Bansal P, Lazo JS. Redox regulation of Cdc25B by cell-active quinolinediones. Mol Pharmacol 2005; 68(6):1810-1820.

19. Campisi J, d'Adda di Fagagna F. Cellular senescence: when bad things happen to good cells. Nat Rev Mol Cell Biol 2007; 8(9):729-740

20. Capasso, A.; Cerchia, C.; Di Giovanni, C.; Granato, G.; Albano, F.; Romano, S.; De Vendittis, E.; Ruocco, M. R.; Lavecchia, A. Ligand-based chemoinformatic discovery of a novel small molecule inhibitor targeting CDC25 dual specificity phosphatases and displaying in vitro efficacy against melanoma cells. Oncotarget 2015; 6(37):40202-22.

21. Cazales M, Schmitt E, Montembault E, Dozier C, Prigent C, Ducommun B.. CDC25B phosphorylation by Aurora-A occurs at the G2/M transition and is inhibited by DNA damage. Cell Cycle 2005; 4(9):1233-1238.

22. Cerchia C, Nasso R, Mori M, Villa S, Gelain A, Capasso A, Aliotta F, Simonetti M, Rullo R, Masullo M, Vendittis E, Ruocco MR and Lavecchia A. Discovery of Novel Naphthylphenylketone and Naphthylphenylamine Derivatives as Cell Division Cycle 25B (CDC25B) Phosphatase Inhibitors: Design, Synthesis, Inhibition Mechanism, and in Vitro Efficacy against Melanoma Cell Lines. J Med Chem 2019; 62(15):7089-7110.

23. Chen M-S, Hurov J, White LS, Woodford-Thomas T and Piwnica-Worms H. Absence of apparent phenotype in mice lacking Cdc25C protein phosphatase. Mol Cell Biol 2001; 21(12):3853-3861.

24. Chen RQ, Yang QK, Lu BW, Yi W, Cantin G, Chen YL, Fearns C, Yates JR, Lee JD. CDC25B mediates rapamycin-Induced oncogenic responses in cancer cells. Cancer Res 2009; 69(6):2663-2668.

25. Cheng L, Lopez-Beltran A, Massari F, MacLennan GT, Montironi R. Molecular testing for BRAF mutations to inform melanoma treatment decisions: a move toward precision medicine. Mod Pathol 2018; 31(1):24-38.

26. Cichorek M, Wachulska M, Stasiewicz A, Tymińska A. Skin melanocytes: biology and development. Postepy Dermatol Alergol 2013; 30(1):30-41.

27. Deibler RW and Kirschner MW. Quantitative reconstitution of mitotic CDK1 activation in somatic cell extracts Mol Cell 2010; 37(6):753-767.

28. Degterev A, Boyce M, Yuan J. A decade of caspases. Oncogene 2003; 22(53):8543-8567.

29. DiPaola RS. To arrest or not to G(2)-M Cell-cycle arrest: commentary re: A. K. Tyagi et al., Silibinin strongly synergizes human prostate carcinoma DU145 cells to doxorubicin-induced growth inhibition, G(2)-M arrest, and apoptosis. Clin Cancer Res 2002; 8(11):3311-3314.

30. Dutertre S, Cazales M, Quaranta M, Froment C, Trabut V, Dozier C, Mirey G, Bouché J-P, Theis-Febvre N, Schmitt E, Monsarrat B, Prigent C, Ducommun B. Phosphorylation of CDC25B by Aurora-A at the centrosome contributes to the G2-M transition. J Cell Sci 2004; 117(12):2523-2531.

31. Evain-Bana E, Schiavo L, Bour C, Lanfranchi DA, Berardozzi S, Ghirga F, Bagrel D, Botta B, Hanquet G, Mori M. Synthesis, biological evaluation and molecular modeling studies on novel quinonoid inhibitors of CDC25 phosphatases. J Enzyme Inhib Med Chem 2017; 32(1):113-118.

32. Feng J, Tamaskovic R, Yang Z, Brazil DP, Merlo A, Hess D, Hemmings BA. Stabilization of Mdm2 via decreased ubiquitination is mediated by protein kinase B/Akt-dependent phosphorylation. J Biol Chem 2004; 279(34):35510-35517.

33. Gabrielli B and Burgess A. Cdc25 Family Phosphatases in Cancer. In: Neel BG, Tonks NK, editors. Protein Tyrosine Phosphatases in Cancer. Springer, New York, NY. 2016; p.283-306.

34. Galaktionov K., Lee A.K., Eckstein J., Draetta G., Meckler J., Loda M., Beach D. CDC25 phosphatases as potential human oncogenes. Science 1995; 269(5230):1575-1577.

35. Gelzo M, Granato G, Albano F, Arcucci A, Dello Russo A, De Vendittis E, Ruocco MR, Corso G. Evaluation of Cytotoxic Effects of 7-Dehydrocholesterol on Melanoma Cells. Free Radic Biol Med 2014; 70:129-140.

36. Gopal YN, Deng W, Woodman SE, et al. Basal and treatment- induced activation of AKT mediates resistance to cell death by AZD6244 (ARRY-142886) in Braf-mutant human cutaneous melanoma cells. Cancer Res 2010; 70(21):8736-8747.

37. Heidenreich E, Eisler H, Steinboeck F. Epistatic participation of REV1 and REV3 in the formation of UV-induced frameshift mutations in cell cycle-arrested yeast cells. Mutat Res 2006; 593(1-2):187-195.

38. Hoffmann I, Clarke PR, Marcote MJ, Karsenti E, Draetta G. Phosphorylation and activation of human cdc25-C by cdc2-cyclin B and its involvement in the self-amplification of MPF at mitosis. EMBO J 1993; 12(1):53-63.

39. Holmes TR, Dindu S, Hansen LA. Aberrant localization of signaling proteins in skin cancer: implications for treatment. Mol Carcinog 2019; 58(9):1631-1639.

40. Horiguchi T, Nishi K, Hakoda S, Tanida S, Nagata A, Okayama H. Dnacin A1 and dnacin B1 are antitumor antibiotics that inhibit cdc25B phosphatase activity.Biochem Pharmacol 1994; 48(11):2139-2141.

41. Ihle MA, Fassunke J, König K, Grünewald I, Schlaak M, Kreuzberg N, Tietze L, Schildhaus H-U, Büttner R and Merkelbach-Bruse S. Comparison of high resolution melting analysis, pyrosequencing, next generation sequencing and immunohistochemistry to conventional Sanger sequencing for the detection of p.V600E and non-p.V600E BRAF mutations. BMC Cancer 2014; 14:13.

42. Irwin JJ, Sterling T, Mysinger MM, Bolstad ES and Coleman RG. ZINC: A Free Tool to Discover Chemistry for Biology. J Chem Inf Model 2012; 52(7):1757-1768.

43. Jackett LA and. Scolyer RA. A Review of Key Biological and Molecular Events Underpinning Transformation of Melanocytes to Primary and Metastatic Melanoma. Cancers (Basel) 2019; 11(12):2041.

44. Kar S, Lefterov IM, Wang M, Lazo JS, Scott CN, Wilcox CS, Carr BI. Binding and inhibition of Cdc25 phosphatases by vitamin K analogues. Biochemistry 2003; 42(35):10490-10497.

45. Kiyokawa H., Ray D. serc Anticancer Agents Med Chem 2008;8(8):832-836.

46. Kristjánsdóttir K and Rudolph J. Cdc25 Phosphatases and Cancer. Chemistry and Biology. Chem Biol 2004; 11(8):1043-1051.

47. Kuske M, Westphal D, Wehner R., Schmitz M, Beissert S, Praetorius C, Meier F, Immunomodulatory effects of BRAF and MEK inhibitors: Implications for Melanoma therapy. Pharmacol Res 2018; 136:151-159.

48. Lavecchia A, Di Giovanni C, Pesapane A, Montuori N, Ragno P, Martucci NM, Masullo M, De Vendittis E, Novellino E. Discovery of New Inhibitors of Cdc25b Dual Specificity Phosphatases by Structure-Based Virtual Screening. J Med Chem 2012; 55(9):4142-4158.

49. Lavecchia A, Giovanni C and Novellino E. CDC25 Phosphatase Inhibitors: An Update. Mini Rev Med Chem 2012; 12(1):62-73.

50. Lazo JS, Nemoto K, Pestell KE, Cooley K, Southwick EC, Mitchell DA, Furey W, Rick Gussio, Zaharevitz DW, Joo B and Wipf P. Identification of a Potent and Selective Pharmacophore for Cdc25 Dual Specificity Phosphatase Inhibitors. Mol Pharmacol 2002; 61(4):720-728.

51. Lazo J S and Wipf P. Is Cdc25 a Druggable Target? Anticancer Agents Med Chem 2008; 8(8):837-842.

52. Lincoln AJ, Wickramasinghe D, Stein P, Schultz RM, Palko ME, De Miguel MP, Tessarollo L and Donovan PJ. Cdc25B phosphatase is required for resumption of meiosis during oocyte maturation. Nat Genet 2002; 30(4):446-449.

53. Lindqvist A, Källström H, Lundgren A, Barsoum E. Rosenthal C.K. Cdc25B cooperates with Cdc25A to induce mitosis but has a unique role in activating cyclin B1-Cdk1 at the centrosome. J Cell Biol 2005; 171(1):35-45.

54. Liu K, Zheng M, Lu R, Du J, Zhao Q, Li Z, Li Y and Zhang S. The role of CDC25C in cell cycle regulation and clinical cancer therapy: a systematic review. Cancer Cell Int 2020; 20:213.

55. Lu M, Breyssens H, Salter V, Zhong S, Hu Y, Baer C, Ratnayaka I, Sullivan A, Brown NR, Endicott J, Knapp S, Kessler BM, Middleton MR, Siebold C, Jones EY, Sviderskaya EV, Cebon J, John T, Caballero OL, Goding CR, Lu X. Restoring p53 Function in Human Melanoma Cells by Inhibiting MDM2 and Cyclin B1/CDK1-Phosphorylated Nuclear iASPP. Cancer Cell 2013; 23(5):618-633.

56. Lugović-Mihić L, Ćesić D, Vuković P, Bilić GN, Šitum M, Špoljar S. Melanoma Development: Current Knowledge on Melanoma Pathogenesis. Acta Dermatovenerol Croat 2019; 27(3):163-168.

57. Maréchal A. and Zou L. DNA damage sensing by the ATM and ATR kinases. Cold Spring Harb Perspect Biol 2013;5(9):a012716.

58. Masyuk TM, Radtke BV, Stroope AJ, Banales JM, Masyuk AI, Gradilone SA, Gajdos GB, Natasha Chandok, Bakeberg JL, Ward CJ, Ritman EL, Kiyokawa H, LaRusso NF. Inhibition of Cdc25A suppresses hepato-renal cystogenesis in rodent models of polycystic kidney and liver disease. Gastroenterology 2012; 142(3):622-633.

59. McGowan C.H., Russell P. The DNA damage response: Sensing and signaling. Curr Opin Cell Biol 2004; 16(6):629-633.

60. Morgan DO. Principles of CDK regulation. Nature 1995; 374(6518):131-134.

61. Niida H and Nakanishi M. DNA damage checkpoints in mammals. Mutagenesis 2006; 21(1):3-9.

62. Perna D, Karreth FA, Rust AG, Perez-Mancera PA, Rashid M, Iorio F, Alifrangis C, Arends MJ, Bosenberg MW, Bollag G, Tuveson DA, Adams DJ. BRAF inhibitor resistance mediated by the AKT pathway in an oncogenic BRAF mouse melanoma model. Proc Natl Acad Sci U S A 2015; 112(6):E536-545.

63. Rabbie R, Ferguson P, Molina-Aguilar C, Adams DJ and Robles-Espinoza CD. Melanoma subtypes: genomic profiles, prognostic molecular markers and therapeutic possibilities. J Pathol 2019; 247(5):539-551.

64. Rafehi H, Orlowski C, Georgiadis GT, Ververis K, El-Osta A, Karagiannis TC. Clonogenic assay: adherent cells. J Vis Exp 2011; 13(49):2573.

65. Reynolds RA, Yem AW, Wolfe CL, Deibel MR, Jr Chidester CG, Watenpaugh KD. Crystal Structure of the Catalytic Subunit of Cdc25b Required for G2/M Phase Transition of the Cell Cycle. J Mol Biol 1999; 293(3):559-568.

66. Rezatabar S, Karimian A, Rameshknia V, Parsian H, Majidinia M, Kopi TA, Bishayee A, Sadeghinia A, Yousefi M, Monirialamdari M and,Yousefi B.. RAS/MAPK signaling functions in oxidative stress, DNA damage response and cancer progression. J Cell Physiol 2019; 234(9), 14951–14965.

67. Rosenkera KMG, Paquettea WD, Johnston PA, Sharlowc ER, Vogt A, Bakand A, Lazo JS, Wipf P. Synthesis and biological evaluation of 3-aminoisoquinolin-1(2H)-one based inhibitors of the dual-specificity phosphatase Cdc25B. Bioorg Med Chem 2015 Jun 15;23(12):2810-2818.

68. Rudolph J. Cdc25 phosphatases: structure, specificity, and mechanism. Biochemistry 2007; 46(12):3595-3604.

69. Ruocco MR, Avagliano A, Granato G, Vigliar E, Masone S, Montagnani S, Arcucci A. Metabolic flexibility in melanoma: A potential therapeutic target. Semin Cancer Biol 2019; 59:187-207.

70. Russell P, Nurse P. Cdc25+ functions as an inducer in the mitotic control of fission yeast. Cell 1986; 45(1):145-153.

71. Sancar A, Lindsey-Boltz LA, Ünsal-Kaçmaz K, Linn S. Molecular mechanisms of mammalian DNA repair and the DNA damage checkpoints. Annu Rev Biochem 2004; 73:39-85.

72. Sato Y, Sasaki H, Kondo S, Fukai I, Kiriyama M, Yamakawa Y, Fujii Y. Expression of the cdc25B mRNA correlated with that of N-myc in neuroblastoma. Jpn J Clin Oncol 2001; 31(9):428-431.

73. Scolyer RA, Longa GV, Thompsona JF. Evolving concepts in melanoma classification and their relevance to multidisciplinary melanoma patient care. Mol Oncol 2011; 5(2):124-136.

74. Serçin Ö, Kemp MG. Characterization of functional domains in human Claspin. Cell Cycle 2011; 10(10):1599-1606.

75. Sexl V, Diehl JA, Sherr CJ, Ashmun R, Beach D, Roussel MF. A rate limiting function of cdc25A for S phase entry inversely correlates with tyrosine dephosphorylation of Cdk2. Oncogene 1999; 18(3):573-582.

76. Shen T, Huang S. The Role of Cdc25A in the Regulation of Cell Proliferation and Apoptosis. Anticancer Agents Med Chem 2012; 12(6):631-639.

77. Sohn J, Kiburz B, Li Z, Deng L, Safi A, Pirrung MC, Rudolph J. Inhibition of Cdc25 Phosphatases by Indolyldihydroxyquinones. J Med Chem 2003; 46(13): 2580-2588.

78. Song Y, Lin X, Kang D, Li X, Zhan P, Liu X, Zhang Q. Discovery and characterization of novel imidazopyridine derivative CHEQ-2 as a potent CDC25 inhibitor and promising anticancer drug candidate. Eur J Med Chem 2014; 23(82):293-307.

79. Sullivan RJ, Flaherty KT. Resistance to BRAF-targeted therapy in melanoma. Eur J Cancer 2013; 49(6):1297-1304.

80. Sur S, Agrawal DK. Phosphatases and kinases regulating CDC25 activity in the cell cycle: clinical implications of CDC25 overexpression and potential treatment strategies. Mol Cell Biochem 2016; 416(1-2):33-46.

81. Suryadinata R, Sadowski M, Sarcevic B. Control of cell cycle progression by phosphorylation of cyclin-dependent kinase (CDK) substrates. Biosci Rep 2010; 30(4):243-255.

82. Szymonowicz K, Oeck., Malewicz N., Jendrossek V. New insights into protein kinase B/Akt signaling: Role of localized akt activation and compartment-specific target proteins for the cellular radiation response. Cancers (Basel) 2018;10(3):78.

83. Tao Y, Hao X, Ding X, Cherukupalli S, Song Y, Liu X, Zhan P. Medicinal chemistry insights into novel CDC25 inhibitors. Eur J Med Chem 2020; 201:112374.

84. Tsao H, Mihm MC, Sheehan C. PTEN expression in normal skin, acquired melanocytic nevi, and cutaneous melanoma. J Am Acad Dermatol 2003; 49(5):865-872.

85. Uzdensky AB, Demyanenko VS, Bibov MY. Signal transduction in human cutaneous melanoma and target drugs. Curr Cancer Drug Targets 2013; 13(8):843-866.

86. Vanella V, Festino L, Trojaniello C, Vitale MG, Sorrentino A, Paone M, Ascierto PA. The Role of BRAF-Targeted Therapy for Advanced Melanoma in the Immunotherapy Era Curr Oncol Rep 2019; 21(9):76.

87. Wang Y, Ji P, Liu J, Broaddus RR, Xue F and Zhang W. Centrosome-associated regulators of the G2/M checkpoint as targets for cancer therapy. Molecular Cancer 2009; 8(8).

88. Wolter KG, Hsu YT, Smith CL, Nechushtan A, Xi X-G, Youle RJ. Movement of Bax from the Cytosol to Mitochondria during Apoptosis. J Cell Biol 1997; 139 (5):1281–1292.

89. Yamaura M, Mitsushita J, Furuta S, Kiniwa Y, Ashida A, Goto Y, Shang WH, Kubodera M, Kato M, Takata M, Saida T, Kamata T. NADPH oxidase 4 contributes to transformation phenotype of melanoma cells by regulating G2-M cell cycle progression. Cancer Res 2009; 69(6):2647-254.

90. Zacksenhaus E, Liu JC, Granieri L, Vorobieva I, Wang D-Y, Ghanbari-Azarnier R, Huiqin Li, Ali A, Chung PED, Ju YJ, Jiang Z, Shrestha M. CDC25 as a common therapeutic target for triple-negative breast cancer – the challenges ahead. Mol Cell Oncol 2018; 5(4):e1481814.

91. Zhou Y, Feng X, Wang L, Du J, Zhou Y, Yu H, Zang Y, Li J, Li J. LGH00031, a novel ortho-quinonoid inhibitor of cell division cycle 25B, inhibits human cancer cells via ROS generation. Acta Pharmacol Sin 2009; 30(9):1359-1368.

92. Zou X, Tsutsui T, Ray D, Blomquist JF, Ichijo H, Ucker DS, Kiyokawa H. The Cell Cycle-Regulatory CDC25A Phosphatase Inhibits Apoptosis Signal-Regulating Kinase 1. Mol Cell Biol 2001; 21(14):4818-4828.

93. Zwergel C, Czepukojc B, Evain-Bana E, Xu Z, Stazia G, Mori M, Patsilinakosahi A, Mai A, Botta B, Ragno R, Bagrel D, Kirsch G, Meiser P,

Jacobc C, Montenarh M, Valente S. Novel coumarin- and quinolinone-based polycycles as cell division cycle 25-A and -C phosphatases inhibitors induce proliferation arrest and apoptosis in cancer cells. Eur J Med Chem 2017; 134:316-333.